

Essentially non-perturbative and peculiar polarization effects in planar QED with strong coupling

Yu. Voronina,^{1,*} K. Sveshnikov,^{1,†} P. Grashin,^{1,‡} and A. Davydov^{1,§}

¹*Department of Physics and Institute of Theoretical Problems of MicroWorld,
Moscow State University, 119991, Leninsky Gory, Moscow, Russia*

(Dated: August 18, 2021)

The essentially non-perturbative polarization effects are considered for a planar supercritical Dirac-Coulomb system with strong coupling (similar to graphene and graphene-based heterostructures) in terms of induced charge density $\rho_{VP}(\vec{r})$. The main attention is paid to the renormalization, convergence of the partial expansion and the behavior of $\rho_{VP}(\vec{r})$ and the integral induced charge Q_{VP} in the overcritical region. The dependence of the induced density on the screening of the Coulomb asymptotics of the external source is also explored in detail. Some peculiar effects in the discrete spectrum with the lowest rotational numbers $m_j = \pm 1/2, \pm 3/2$ in the screened case are detected and their possible role in the transition through corresponding Z_{cr} is also discussed.

PACS numbers: 12.20.Ds, 31.30.J-, 31.30.jf, 81.05.ue

Keywords: non-perturbative QED effects, 2+1 QED with strong coupling, graphene and graphene-based heterostructures, induced charge density, screening effects

1. INTRODUCTION

There is now a lot of interest to the study of various 2+1 QED-effects in graphene-based planar heterostructures. It is known that the charge carriers in graphene are described as massless (or massive on a substrate) relativistic fermions, what leads to an intriguing analogy between the physics of graphene and that of QED. Moreover, the effective fine-structure constant $\alpha_g \sim 1$ in graphene turns out to be much larger than in the “normal” 3+1 QED [1],[2]. Due to such a large value of α_g it is much easier to observe many non-trivial QED-effects experimentally. In particular, the critical charges of atomic collapse in graphene are subject of condition $Z\alpha_g > 1/2$ [3],[4], the observation of the Klein paradox requires electric fields $\sim 10^5$ V/cm (eleven orders of magnitude less than the fields necessary for the observation of the Klein paradox for elementary particles) [5], the quantum Hall effect can be observed for much higher temperatures and lower magnetic fields than in the conventional semiconductors [6–8]. Some effects turn out to be strong enough to affect the transport properties of graphene. For instance, highly charged impurities in graphene exhibit resonances which should manifest themselves via various transport properties, such as the transport scattering cross-section [3]. The Klein paradox plays an important role in transport properties of different graphene systems [5]: graphene p-n-p junctions [3],[9], twisted graphene bilayer [10]. The Dirac-like dynamics of graphene results also in an unconventional form of the Hall quantization [6]. The main feature inherent in all these effects is that they are essentially non-perturbative due to the large

value of α_g and therefore cannot be described within the perturbation theory (PT).

In this work we explore another essentially non-perturbative effect in the two-dimensional strongly coupled QED with application to graphene-like planar systems, namely, the vacuum polarization, caused by diving of discrete levels into the lower continuum in the supercritical static or adiabatically slowly varying Coulomb fields, which are created by localized extended sources with $Z > Z_{cr}$. Such effects have attracted a considerable amount of theoretical and experimental activity in 3+1 D heavy ions collisions, where for $Z > Z_{cr,1} \simeq 170$ a non-perturbative reconstruction of the vacuum state is predicted, which should be accompanied by a number of nontrivial effects including the vacuum positron emission ([11–15] and refs. therein).

Similar phenomena could occur in graphene with the charge impurities acting as atomic nuclei, while the graphene itself – as the QED vacuum and its electrons and holes — as the relativistic virtual particles which populate the vacuum. A remarkable circumstance here is that due to the large value of the effective fine-structure constant these effects should take place for relatively small impurity charges $Z \simeq 1 - 10$. Since for these effects the charge carriers in graphene play the role of the virtual QED-particles, the induced charge density can be measured directly. In Ref. [16], the five-dimer cluster consisting of Ca-atoms was used as a charge impurity and the induced density was measured via STM. Polarization effects in graphene, caused by charged impurities, have also been considered by many authors ([17–23] and refs. therein). Here it should be noted that in most cases the impurity is modeled as a point-like charge, what causes some problems in the supercritical case. Our work is aimed mainly at the study of vacuum polarization effects, caused by extended supercritical Coulomb sources with non-zero size R_0 , which provide a physically clear and unambiguous problem statement like in Refs. [4, 24, 25], where the charge is assumed to be displaced away or

*Electronic address: voroninayu@physics.msu.ru

†Electronic address: costa@bog.msu.ru

‡Electronic address: grashin.petr@physics.msu.ru

§Electronic address: davydov.andrey@physics.msu.ru

smearing over a finite region of the graphene plane.

The external Coulomb field $A_0^{ext}(\vec{r})$ is chosen in the form of a projection onto a plane of the potential of the uniformly charged sphere with the radius R_0 and a cutoff of the Coulomb asymptotics at some $R_1 > R_0$

$$A_0^{ext}(\vec{r}) = Z|e| \left[\frac{1}{R_0} \theta(R_0 - r) + \frac{1}{r} \theta(R_0 \leq r \leq R_1) \right], \quad (1)$$

what leads to the potential energy

$$V(r) = -Z\alpha \left[\frac{1}{R_0} \theta(R_0 - r) + \frac{1}{r} \theta(R_0 \leq r \leq R_1) \right]. \quad (2)$$

The radius of the source is taken as $R_0 = a$, where $a \simeq 1.42 A$ is the approximate C-C distance in the graphene lattice. Such cutoff of the Coulomb potential at small distances has been used in [26]. The cutoffs $R_0 = a/2$ and $R_0 = 2a$ are also considered. The screening of the Coulomb asymptotics is taken in the form the simplest shielding via vertical wall for $r \geq R_1 > R_0$, which allows to perform the most part of calculations in the analytical form. However, even such type of screening reveals some peculiar features, which are quite different from the unscreened one and are absent in the similar one- or three-dimensional DC systems. The external cutoff R_1 will be taken as $R_1 = 2R_0, 5R_0, 10R_0, \infty$ for the study of screening effects and to establish a smooth transition into the unscreened case, which will be considered at first.

The effective fine-structure constant is defined as

$$\alpha = e^2 / (\hbar v_F \varepsilon_{eff}), \quad \varepsilon_{eff} = (\varepsilon + 1)/2, \quad (3)$$

with ε being the substrate dielectric constant and $v_F = 3ta/2\hbar$ – the Fermi velocity in graphene. In its turn, t is the hopping amplitude, while $\lambda_c = \hbar/mv_F$ is the effective Compton length [27]. Here m denotes the effective fermion mass, which is related to the local energy mismatch in the tight-binding formulation through the relation $\Delta = 2mv_F^2$. These definitions lead to the relation $\lambda_c/a \simeq 3t/\Delta$. In this work we consider $\alpha = 0.4$ (which corresponds to graphene on the SiC substrate [26]) and $\alpha = 0.8$ (graphene on the h-BN substrate [27, 28]).

Henceforth the system of units in which $\hbar = v_F = m = 1$ is used, and so the distances are measured in units of λ_c , while the energy — in units of mv_F^2 . For $\alpha = 0.4$ the local energy mismatch is $\Delta = 0.26$ eV and therefore for $R_0 = a/2, a, 2a$ one obtains $R_0 = 1/60, 1/30, 1/15$ in the units chosen, while for $\alpha = 0.8$ one has $\Delta = 0.056$ eV and so $R_0 = 1/350, 1/175, 2/175$.

2. THE PERTURBATIVE APPROACH TO 2+1 QED FOR AN EXTENDED COULOMB SOURCE WITH UNSCREENED ASYMPTOTICS

In 2+1 QED the induced charge density to the lowest order of PT is determined from the vacuum polarization (Uehling) potential

$$\rho_{VP}^{(1)}(\vec{r}) = -\frac{1}{4\pi} \Delta_2 A_{VP,0}^{(1)}(\vec{r}), \quad (4)$$

where Δ_2 is the two-dimensional Laplace operator. In its turn, the Uehling potential $A_{VP,0}^{(1)}$ is expressed in terms of the renormalized polarization function $\Pi_R(-\vec{q}^2)$ and the Coulomb potential of external source in the momentum space $\tilde{A}_0(\vec{q})$ [14]

$$A_{VP,0}^{(1)}(\vec{r}) = \frac{1}{(2\pi)^2} \int d^2q e^{i\vec{q}\vec{r}} \Pi_R(-q^2) \tilde{A}_0(\vec{q}), \quad (5)$$

$$\tilde{A}_0(\vec{q}) = \int d^2r' e^{-i\vec{q}\vec{r}'} A_0^{ext}(\vec{r}'), \quad q = |\vec{q}|,$$

where

$$\Pi_R(-q^2) = \frac{\alpha}{2q} \left[\frac{2}{q} + \left(1 - \frac{4}{q^2} \right) \arctan\left(\frac{q}{2}\right) \right], \quad (6)$$

and the two-dimensional representation of the Dirac matrices has been used (for the choice of the Dirac matrices see below in Section 3).

From (5), (6) for the external source (1) one obtains the following expression for the Uehling potential

$$A_{VP,0}^{(1)}(r) = \frac{Z\alpha|e|}{4} \int_0^\infty dq \frac{J_0(qr)}{q} \left[\frac{2}{q} + \left(1 - \frac{4}{q^2} \right) \times \right. \\ \left. \times \arctan\left(\frac{q}{2}\right) \right] \times (2[1 + J_1(qR_0) - qR_0J_0(qR_0)] + \\ + \pi qR_0 [J_0(qR_0)\mathbf{H}_1(qR_0) - J_1(qR_0)\mathbf{H}_0(qR_0)]) \quad (7)$$

with $J_\nu(z)$ and $\mathbf{H}_\nu(z)$ being the Bessel and Struve functions, correspondingly. From (4) and (7) the first-order perturbative induced density $\rho_{VP}^{(1)}$ can be calculated. In order to figure out whether it is possible to insert the Laplace operator under the integral over dq in (7) let us consider the asymptotical behavior of the integrand for large q . The leading term of the integrand asymptotics in (7) equals to

$$\frac{\sin(q(r + R_0)) + \cos(q(r - R_0))}{\sqrt{r}R_0^{3/2}q^3}, \quad q \rightarrow \infty. \quad (8)$$

Applying the Laplace operator to (8), to the leading order one obtains

$$-\frac{\sin(q(r + R_0)) + \cos(q(r - R_0))}{\sqrt{r}R_0^{3/2}q} + O(1/q^2). \quad (9)$$

Therefore, at $r = R_0$ the possibility of inserting the Laplace operator under the sign of the integral in (7) is absent, since in this case the integral over dq in (7) diverges logarithmically.

So the vacuum density, obtained from (4)

$$\rho_{VP}^{(1)}(r) = \frac{Z\alpha|e|}{16\pi} \int_0^\infty dq q J_0(qr) \left[\frac{2}{q} + \left(1 - \frac{4}{q^2} \right) \times \right. \\ \left. \times \arctan\left(\frac{q}{2}\right) \right] \times (2[1 + J_1(qR_0) - qR_0J_0(qR_0)] + \\ + \pi qR_0 [J_0(qR_0)\mathbf{H}_1(qR_0) - J_1(qR_0)\mathbf{H}_0(qR_0)]) , \quad (10)$$

is finite for all $r \neq R_0$ with the logarithmic singularity at $r \rightarrow R_0$.

By means of the QED-renormalization condition $\tilde{\Pi}_R(q^2) \sim q^2$ for $q \rightarrow 0$ it is easy to verify that within PT to the leading order the total induced charge vanishes exactly

$$\int d^2r \rho_{VP}^{(1)}(r) = 0 \quad (11)$$

(for more details see [29], App.B). The relation (11) confirms the assumption that for the external background like (1) in the subcritical region with $Z < Z_{cr,1}$ the correctly renormalized total induced charge should vanish, while the polarization effects could only distort its spatial density [14, 30]. However, it is not a theorem, but just a plausible statement, which in any concrete case should be verified via direct calculations. In the case under consideration the direct check confirms (see [29], App.B) that upon renormalization the induced charge turns out to be non-vanishing only for $Z > Z_{cr,1}$ due to non-perturbative effects, caused by diving of discrete levels into the lower continuum in accordance with Refs. [11, 12, 14, 15]. This circumstance significantly affects the behavior of the Casimir energy in the overcritical region, which has been recently shown for a toy 2+1 D model in [31], and will be considered for DC system with current parameters in a separate work.

3. THE WICHMANN-KROLL METHOD FOR THE INDUCED DENSITY IN THE UNSCREENED COULOMB BACKGROUND

The most effective non-perturbative approach to calculation of the induced density $\rho_{VP}(\vec{r})$ is based on the Wichmann-Kroll (WK) method [32]. The starting point of the WK method is the following expression for the induced density

$$\rho_{VP}(\vec{r}) = -\frac{|e|}{2} \left(\sum_{\epsilon_n < \epsilon_F} \psi_n(\vec{r})^\dagger \psi_n(\vec{r}) - \sum_{\epsilon_n \geq \epsilon_F} \psi_n(\vec{r})^\dagger \psi_n(\vec{r}) \right), \quad (12)$$

with ϵ_F being the Fermi level, which in such problems with the external background like (1) should be chosen at the threshold of the lower continuum ($\epsilon_F = -1$), while ϵ_n and $\psi_n(\vec{r})$ are the eigenvalues and the eigenfunctions of corresponding Dirac-Coulomb (DC) spectral problem.

The essence of the WK method is that the induced density (12) is expressed via integration of the trace of the Green function for DC spectral problem along the special contours in the complex energy plane. The Green function is defined as

$$(-i \vec{\alpha} \vec{\nabla} + V(r) + \beta - \epsilon) G(\vec{r}, \vec{r}'; \epsilon) = \delta(\vec{r} - \vec{r}'). \quad (13)$$

Here it should be mentioned that in 2+1 QED the Dirac matrices can be chosen either in two- or four-dimensional representations. In the first case there are two inequivalent possible choices of the matrix signature [33], while

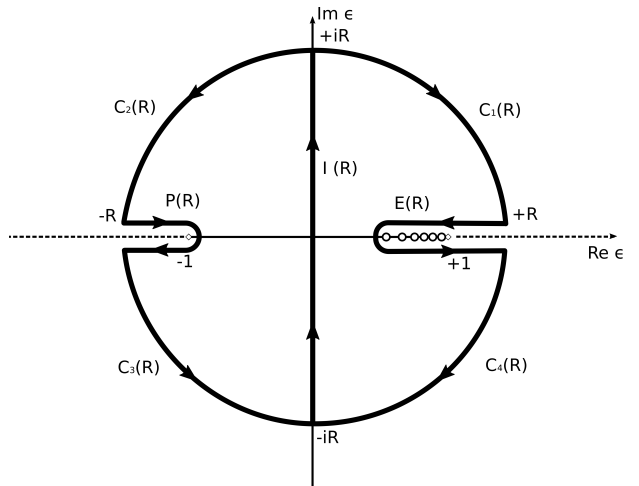


FIG. 1: Special contours in the complex energy plane, used for representation of the vacuum charge density via contour integrals. The direction of contour integration is chosen in correspondence with (14).

in the latter the DC spectral problem for the external source (1) splits into two independent subsystems, which are related by $m_j \rightarrow -m_j$. Therefore the degeneracy factor of the energy eigenstates with the fixed m_j equals to 2 and in what follows this factor will be shown explicitly in all the expressions for $\rho_{VP}(\vec{r})$ and \mathcal{E}_{VP} , while the DC spectral problem without any loss of generality can be considered in the two-dimensional representation with $\alpha_i = \sigma_i$, $\beta = \sigma_3$.

The formal solution of (13) is written as

$$G(\vec{r}, \vec{r}'; \epsilon) = \sum_n \frac{\psi_n(\vec{r}) \psi_n(\vec{r}')^\dagger}{\epsilon_n - \epsilon}. \quad (14)$$

Following [32], the induced density is expressed via the integrals along the contours $P(R)$ and $E(R)$ on the first sheet of the Riemann energy surface (Fig.1)

$$\rho_{VP}(\vec{r}) = -\frac{|e|}{2} \lim_{R \rightarrow \infty} \left(\frac{1}{2\pi i} \int_{P(R)} d\epsilon \text{Tr} G(\vec{r}, \vec{r}; \epsilon) + \frac{1}{2\pi i} \int_{E(R)} d\epsilon \text{Tr} G(\vec{r}, \vec{r}; \epsilon) \right). \quad (15)$$

Since the DC spectral problem in the external field (1) divides into radial and angular parts via substitution

$$\psi(\vec{r}) = \frac{1}{\sqrt{2\pi}} \begin{pmatrix} i\psi_1(r) e^{i(m_j - 1/2)\varphi} \\ \psi_2(r) e^{i(m_j + 1/2)\varphi} \end{pmatrix}, \quad (16)$$

for the trace of the Green function (14) one obtains

$$\begin{aligned} \text{Tr}G(\vec{r}, \vec{r}; \epsilon) &= \frac{1}{2\pi} \text{Tr}G(r, r; \epsilon) = \\ &= \frac{1}{2\pi} \left(2 \sum_{m_j=\pm 1/2, \pm 3/2, \dots} \text{Tr}G_{m_j}(r, r; \epsilon) \right), \quad (17) \\ \text{Tr}G_{m_j}(r, r; \epsilon) &= \frac{1}{J_{m_j}(\epsilon)} \psi_{m_j}^{in}(r)^T \psi_{m_j}^{out}(r), \end{aligned}$$

where $\psi_{m_j}^{in}(r)$ and $\psi_{m_j}^{out}(r)$ are the solutions of the radial DC problem for the given m_j , which are regular at $r = 0$ and $r = +\infty$ correspondingly, with $J_{m_j}(\epsilon)$ being their Wronskian

$$J_{m_j}(\epsilon) = [\psi_{m_j}^{in}, \psi_{m_j}^{out}]. \quad (18)$$

In (18) and in what follows we use the following denotation

$$[f, g]_a = a(f_2(a)g_1(a) - f_1(a)g_2(a)).$$

Such definition of $\text{Tr}G_{m_j}$ provides its correct normalization. It should be noted that the zeros of $J_{m_j}(\epsilon)$, lying on the first sheet, are real-valued and correspond to the discrete spectrum, while those on the second sheet become complex conjugate pairs and define the positions of elastic resonances.

Proceeding further, let us construct $\text{Tr}G_{m_j}$ for the external potential (1). For the given m_j the radial DC problem takes the following form

$$\begin{cases} \frac{d}{dr} \psi_1(r) + \frac{1/2 - m_j}{r} \psi_1(r) = (\epsilon - V(r) + 1) \psi_2(r), \\ \frac{d}{dr} \psi_2(r) + \frac{1/2 + m_j}{r} \psi_2(r) = -(\epsilon - V(r) - 1) \psi_1(r). \end{cases} \quad (19)$$

For $0 \leq r \leq R_0$ the linearly independent solutions of (19) are chosen in the form

$$\begin{aligned} \text{for } \psi_1(r): \quad \mathcal{I}_1(r) &= \xi I_{|m_j-1/2|}(\xi r), \\ \mathcal{K}_1(r) &= -\xi K_{|m_j-1/2|}(\xi r); \\ \text{for } \psi_2(r): \quad \mathcal{I}_2(r) &= (1 - \epsilon - V_0) I_{|m_j+1/2|}(\xi r), \\ \mathcal{K}_2(r) &= (1 - \epsilon - V_0) K_{|m_j+1/2|}(\xi r). \end{aligned} \quad (20)$$

In (20) $I_\nu(z)$ and $K_\nu(z)$ are the modified Bessel functions of the first and second kind, respectively,

$$V_0 = Z\alpha/R_0, \quad \xi = \sqrt{1 - (\epsilon + V_0)^2}, \quad \text{Re } \xi \geq 0. \quad (21)$$

For $r > R_0$ the fundamental pair of solutions for the system (19) is taken as

$$\begin{aligned} \text{for } \psi_1(r): \\ \mathcal{M}_1(r) &= \frac{1 + \epsilon}{r} [(\varkappa - \nu) M_{\nu-1/2, \varkappa}(2\gamma r) + \\ &+ \left(m_j + \frac{Q}{\gamma}\right) M_{\nu+1/2, \varkappa}(2\gamma r)], \\ \mathcal{W}_1(r) &= \frac{1 + \epsilon}{r} \left[\left(m_j - \frac{Q}{\gamma}\right) W_{\nu-1/2, \varkappa}(2\gamma r) - \right. \\ &\left. - W_{\nu+1/2, \varkappa}(2\gamma r) \right]; \end{aligned}$$

for $\psi_2(r)$:

$$\begin{aligned} \mathcal{M}_2(r) &= \frac{\gamma}{r} [(\varkappa - \nu) M_{\nu-1/2, \varkappa}(2\gamma r) - \\ &- \left(m_j + \frac{Q}{\gamma}\right) M_{\nu+1/2, \varkappa}(2\gamma r)], \\ \mathcal{W}_2(r) &= \frac{\gamma}{r} \left[\left(m_j - \frac{Q}{\gamma}\right) W_{\nu-1/2, \varkappa}(2\gamma r) + \right. \\ &\left. + W_{\nu+1/2, \varkappa}(2\gamma r) \right], \quad (22) \end{aligned}$$

where $M_{b,c}(z)$ and $W_{b,c}(z)$ are the Whittaker functions [34],

$$\begin{aligned} Q &= Z\alpha, \quad \varkappa = \sqrt{m_j^2 - Q^2}, \quad \nu = \frac{\epsilon Q}{\gamma}, \\ \gamma &= \sqrt{1 - \epsilon^2}, \quad \text{Re } \gamma \geq 0. \end{aligned} \quad (23)$$

Proceeding further, $\psi_{m_j}^{in}(r)$ and $\psi_{m_j}^{out}(r)$ are chosen as such linear combinations of the solutions (20) and (22), which are regular at $r = 0$ and $r = +\infty$, correspondingly.

As a result, the expression for $\text{Tr}G_{m_j}$ takes the form

$$\begin{aligned} \text{Tr}G_{m_j}(r, r; \epsilon) &= \\ &= \frac{1}{[\mathcal{I}, \mathcal{K}]} \left(\mathcal{I}_1 \mathcal{K}_1 + \mathcal{I}_2 \mathcal{K}_2 - \frac{[\mathcal{K}, \mathcal{W}]_{R_0}}{[\mathcal{I}, \mathcal{W}]_{R_0}} (\mathcal{I}_1^2 + \mathcal{I}_2^2) \right) \theta(R_0 - r) + \\ &+ \frac{1}{[\mathcal{M}, \mathcal{W}]} \left(\mathcal{M}_1 \mathcal{W}_1 + \mathcal{M}_2 \mathcal{W}_2 - \frac{[\mathcal{I}, \mathcal{M}]_{R_0}}{[\mathcal{I}, \mathcal{W}]_{R_0}} (\mathcal{W}_1^2 + \mathcal{W}_2^2) \right) \times \\ &\quad \times \theta(r - R_0), \quad (24) \end{aligned}$$

where

$$[\mathcal{M}, \mathcal{W}] = -4(1 + \epsilon) \gamma^2 \frac{\Gamma(2\varkappa + 1)}{\Gamma(\varkappa - \nu)}, \quad [\mathcal{I}, \mathcal{K}] = \epsilon + V_0 - 1, \quad (25)$$

while the Wronskian (18), which enters into the expression for $\text{Tr}G_{m_j}$ (17), equals to

$$J_{m_j}(\epsilon) = [\mathcal{I}, \mathcal{W}]_{R_0}. \quad (26)$$

In the next step one finds the asymptotics of $\text{Tr}G_{m_j}$ on the arcs of the large circle in the upper half-plane (Fig.1) $C_1(R)$ and $C_2(R)$, where $|\epsilon| \rightarrow \infty$, $0 < \text{Arg } \epsilon < \pi$:

$$\begin{aligned} \text{Tr}G_{m_j}(r, r; \epsilon) &\rightarrow \\ &\rightarrow \frac{i}{r} + \frac{i}{2r\epsilon^2} \left(\frac{m_j^2}{r^2} + 1 \right) - \frac{i}{r^2\epsilon^3} \left(\frac{m_j^2}{r} V_0 + \frac{m_j}{2r} + rV_0 \right) + \\ &\quad + O(|\epsilon|^{-4}), \quad r < R_0, \\ &\rightarrow \frac{i}{r} + \frac{i}{2r\epsilon^2} \left(\frac{m_j^2}{r^2} + 1 \right) - \frac{i}{r^2\epsilon^3} \left(\frac{m_j^2}{r} \frac{Q}{r} + \frac{m_j}{2r} + Q \right) + \\ &\quad + O(|\epsilon|^{-4}), \quad r > R_0, \quad (27) \end{aligned}$$

and on the arcs of the large circle in the lower half-plane

$C_3(R)$ and $C_4(R)$, where $|\epsilon| \rightarrow \infty$, $-\pi < \text{Arg } \epsilon < 0$:

$$\begin{aligned} & \text{Tr}G_{m_j}(r, r; \epsilon) \rightarrow \\ & \rightarrow -\frac{i}{r} - \frac{i}{2r\epsilon^2} \left(\frac{m_j^2}{r^2} + 1 \right) + \frac{i}{r^2\epsilon^3} \left(\frac{m_j^2}{r} V_0 + \frac{m_j}{2r} + rV_0 \right) + \\ & \quad + O(|\epsilon|^{-4}), \quad r < R_0, \\ & \rightarrow -\frac{i}{r} - \frac{i}{2r\epsilon^2} \left(\frac{m_j^2}{r^2} + 1 \right) + \frac{i}{r^2\epsilon^3} \left(\frac{m_j^2}{r} \frac{Q}{r} + \frac{m_j}{2r} + Q \right) + \\ & \quad + O(|\epsilon|^{-4}), \quad r > R_0. \end{aligned} \quad (28)$$

There follows from (27) and (28) that the integration along the contours $P(R)$ and $E(R)$ in (15) can be reduced to the imaginary axis, whence one finds the final expression for the induced density

$$\rho_{VP}(r) = 2 \sum_{m_j=1/2, 3/2, \dots} \rho_{VP, |m_j|}(r), \quad (29)$$

where

$$\rho_{VP, |m_j|}(r) = \frac{|e|}{(2\pi)^2} \int_{-\infty}^{\infty} dy \text{Tr}G_{|m_j|}(r, r; iy),$$

$$\text{Tr}G_{|m_j|}(r, r; iy) = \text{Tr}G_{m_j}(r, r; iy) + \text{Tr}G_{-m_j}(r, r; iy). \quad (30)$$

In presence of negative discrete levels with $-1 \leq \epsilon_n < 0$

$$\begin{aligned} \rho_{VP, |m_j|}(r) = \frac{|e|}{2\pi} & \left[\sum_{m_j=\pm|m_j|} \sum_{-1 \leq \epsilon_n < 0} \psi_{n, m_j}(r)^\dagger \psi_{n, m_j}(r) + \right. \\ & \left. + \frac{1}{2\pi} \int_{-\infty}^{+\infty} dy \text{Tr}G_{|m_j|}(r, r; iy) \right]. \end{aligned} \quad (31)$$

Proceeding further, let us mention the general property of $\text{Tr}G_{m_j}$ under the change of the sign of external field ($Q \rightarrow -Q$) and complex conjugation

$$\begin{aligned} \text{Tr}G_{-m_j}(Q; r, r; \epsilon) &= -\text{Tr}G_{m_j}(-Q; r, r; -\epsilon), \\ \text{Tr}G_{m_j}(Q; r, r; \epsilon)^* &= \text{Tr}G_{m_j}(Q; r, r; \epsilon^*), \end{aligned} \quad (32)$$

and the direct consequence of these two properties

$$\text{Tr}G_{m_j}(Q; r, r; iy)^* = -\text{Tr}G_{-m_j}(-Q; r, r; iy), \quad (33)$$

whence it follows that $\rho_{VP, |m_j|}(r)$ can be expressed in terms of $\text{Re Tr}G_{|m_j|}(Q; r, r; iy)$ and is definitely a real function being odd in Q (in the full agreement with the Furry theorem). In the purely perturbative region the representation of $\rho_{VP}(r)$ as an odd series in powers of external field (1) is given by the Born series $G_{m_j} = G_{m_j}^{(0)} + G_{m_j}^{(0)}(-V)G_{m_j}^{(0)} + G_{m_j}^{(0)}(-V)G_{m_j}^{(0)}(-V)G_{m_j}^{(0)} + \dots$, whence

$$\begin{aligned} \text{Re Tr}G_{m_j}(r, r; iy) &= \\ &= \sum_{k=0}^{\infty} \text{Re Tr} \left[G_{m_j}^{(0)} \left(-V G_{m_j}^{(0)} \right)^{2k+1} (r, r; iy) \right], \end{aligned} \quad (34)$$

where $G_{m_j}^{(0)}$ is the free Green function of the corresponding radial Dirac equation. At the same time, in presence of negative discrete levels and especially in the overcritical region with $Z > Z_{cr,1}$ $\rho_{VP}(r)$ is still an odd function in Q [35], but now the dependence on the external field cannot be described by the series (34) any more, since there appear in $\rho_{VP}(r)$ essentially nonperturbative and so non-analytic in Q components.

The expression for the induced density (29)-(31) requires renormalization, since there follows from the asymptotics of $\text{Tr}G_{m_j}$

$$\text{Tr}G_{m_j}(r, r; iy) \rightarrow \frac{iy}{\sqrt{1+y^2}} \frac{1}{r} + \frac{Q}{(1+y^2)^{3/2}} \frac{1}{r^2} + O\left(\frac{1}{r^3}\right), \quad r \rightarrow \infty, \quad (35)$$

that the non-renormalized $\rho_{VP}(r)$ decreases for $r \rightarrow \infty$ as $1/r^2$, and so the total induced charge diverges logarithmically.

The general result, obtained in [35] via expression of $\rho_{VP}(r)$ in powers of Q , which is valid for any number of spatial dimensions in the external fields like (1), is that all the divergences of $\rho_{VP}(r)$ originate from the fermionic loop with two external lines, while the next-to-leading orders of expansion are finite. So for calculation of the renormalized induced density ρ_{VP}^{ren} the linear in Q terms should be extracted from $\text{Tr}G_{m_j}$ (24) and replaced by $\rho_{VP}^{(1)}$ (10), which is nonzero only for $|m_j| = 1/2$. For these purposes one finds first the component of the induced density $\rho_{VP, |m_j|}^{(3+)}$ (r), defined as

$$\rho_{VP, |m_j|}^{(3+)}(r) = \frac{|e|}{2\pi} \left[\sum_{m_j=\pm|m_j|} \sum_{-1 \leq \epsilon_n < 0} \psi_{n, m_j}(r)^\dagger \psi_{n, m_j}(r) + \frac{1}{\pi} \int_0^\infty dy \text{Re} \left(\text{Tr}G_{|m_j|}(r, r; iy) - 2 \text{Tr}G_{m_j}^{(1)}(r; iy) \right) \right], \quad (36)$$

where $G_{m_j}^{(1)} = Q \partial G_{m_j} / \partial Q|_{Q=0}$ and can be found through the first Born approximation $G_0(-V)G_0$, which for $r \leq R_0$

gives

$$\begin{aligned} \text{Tr}G_{m_j}^{(1)}(r; iy) = & \frac{Q}{(iy-1)^2} \left[\left(\tilde{\gamma}^2 K_{|m_j-1/2|}^2(\tilde{\gamma}r) + (1-iy)^2 K_{|m_j+1/2|}^2(\tilde{\gamma}r) \right) \int_0^r dr' \frac{r'}{R_0} \left(\tilde{\gamma}^2 I_{|m_j-1/2|}^2(\tilde{\gamma}r') + \right. \right. \\ & \left. \left. + (1-iy)^2 I_{|m_j+1/2|}^2(\tilde{\gamma}r') \right) + \left(\tilde{\gamma}^2 I_{|m_j-1/2|}^2(\tilde{\gamma}r) + (1-iy)^2 I_{|m_j+1/2|}^2(\tilde{\gamma}r) \right) \times \right. \\ & \times \left\{ \int_r^{R_0} dr' \frac{r'}{R_0} \left(\tilde{\gamma}^2 K_{|m_j-1/2|}^2(\tilde{\gamma}r') + (1-iy)^2 K_{|m_j+1/2|}^2(\tilde{\gamma}r') \right) + \right. \\ & \left. \left. + \int_{R_0}^{\infty} dr' \left(\tilde{\gamma}^2 K_{|m_j-1/2|}^2(\tilde{\gamma}r') + (1-iy)^2 K_{|m_j+1/2|}^2(\tilde{\gamma}r') \right) \right\} \right], \end{aligned} \quad (37)$$

and for $r > R_0$

$$\begin{aligned} \text{Tr}G_{m_j}^{(1)}(r; iy) = & \frac{Q}{(iy-1)^2} \left[\left(\tilde{\gamma}^2 K_{|m_j-1/2|}^2(\tilde{\gamma}r) + (1-iy)^2 K_{|m_j+1/2|}^2(\tilde{\gamma}r) \right) \left\{ \int_0^{R_0} dr' \frac{r'}{R_0} \left(\tilde{\gamma}^2 I_{|m_j-1/2|}^2(\tilde{\gamma}r') + \right. \right. \right. \\ & \left. \left. \left. + (1-iy)^2 I_{|m_j+1/2|}^2(\tilde{\gamma}r') \right) + \int_{R_0}^r dr' \left(\tilde{\gamma}^2 I_{|m_j-1/2|}^2(\tilde{\gamma}r') + (1-iy)^2 I_{|m_j+1/2|}^2(\tilde{\gamma}r') \right) \right\} + \right. \\ & \left. + \left(\tilde{\gamma}^2 I_{|m_j-1/2|}^2(\tilde{\gamma}r) + (1-iy)^2 I_{|m_j+1/2|}^2(\tilde{\gamma}r) \right) \int_r^{\infty} dr' \left(\tilde{\gamma}^2 K_{|m_j-1/2|}^2(\tilde{\gamma}r') + \right. \right. \\ & \left. \left. + (1-iy)^2 K_{|m_j+1/2|}^2(\tilde{\gamma}r') \right) \right], \end{aligned} \quad (38)$$

where $\tilde{\gamma} = \sqrt{1+y^2}$. The integrals, containing in the expressions for $\text{Tr}G_{m_j}^{(1)}$ (37) and (38), are not given explicitly due to their cumbersome form.

So the expression for renormalized induced density takes the form

$$\rho_{VP}^{ren}(r) = 2 \left[\rho_{VP}^{(1)}(r) + \sum_{m_j=1/2, 3/2, \dots} \rho_{VP, |m_j|}^{(3+)}(r) \right], \quad (39)$$

where $\rho_{VP}^{(1)}(r)$ is the perturbative induced density (10), evaluated by means of the polarization function (6) in the first order of PT. Such expression for $\rho_{VP}^{ren}(r)$ guarantees the vanishing total induced charge $Q_{VP}^{ren} = \int d^2r \rho_{VP}^{ren}(r)$ for $Z < Z_{cr,1}$, since $Q_{VP}^{(1)}$ is zero by construction, while the subsequent direct calculation confirms that the contribution of $\rho_{VP, |m_j|}^{(3+)}(r)$ to Q_{VP}^{ren} for $Z < Z_{cr,1}$ vanishes too. Unlike 1+1 D, in 2+1 D such a check cannot be performed in the purely analytical form any more due to complexity of expressions, containing in $\rho_{VP, |m_j|}^{(3+)}(r)$. Nevertheless, it could be quite reliably performed via special combination of analytical and numerical methods ([29], App.B). Moreover, it suffices to verify the disappearance of the total charge Q_{VP}^{ren} not for the entire subcritical region, but only in absence of negative discrete levels. In presence of the latter, the vanishing total charge for $Z < Z_{cr,1}$ follows from model-independent ar-

guments, which are based on the starting expression for the induced density (12). Namely, there follows from (12) that the change of the integral induced charge is possible for $Z > Z_{cr,1}$ only, when the discrete levels attain the lower continuum. Moreover, upon diving into the lower continuum each doubly degenerate energy level yields the change of the integral charge exactly by $(-2|e|)$. One of the possible correct ways to prove this statement is given in Ref. [36]. Let us specially mention that this effect is essentially non-perturbative and completely included in $\rho_{VP}^{(3+)}$, while $\rho_{VP}^{(1)}$ does not participate in it and still makes an exactly vanishing contribution to the total charge. Thus, the behavior of the renormalized by means of (39) induced density in the non-perturbative region turns out to be indeed such that should be expected from the general assumptions about the structure of the electron-positron (or electron-hole in our context) vacuum for $Z > Z_{cr}$ [11, 12, 14, 15].

A more detailed picture of these changes in $\rho_{VP}^{ren}(r)$ is quite similar to that considered in [11, 12, 14, 15] for 3+1 QED by means of U.Fano approach [37]. The main result is that any discrete level $\psi_{n, m_j}(r)$, dived into the lower continuum, yields the change of the induced density by

$$\Delta\rho_{VP}(r) = -2|e|\psi_{n, m_j}(r)^\dagger \psi_{n, m_j}(r)|_{\epsilon_n=-1}. \quad (40)$$

The next point is that the renormalized induced density (39) is represented by an infinite sum over m_j . So

the convergence of this sum should be explored in detail. For these purposes let us consider the asymptotics of $\rho_{VP,|m_j|}^{(3+)}(r)$ (36) for large $|m_j|$. The asymptotics of $\text{Tr}G_{m_j}(r, r; iy)$ (24) for $|m_j| \rightarrow \infty$ takes the form

$$\begin{aligned} \text{Tr}G_{m_j}(r, r; iy) &\rightarrow \\ &\rightarrow \frac{iy + V_0}{|m_j|} + \frac{\text{sgn}(m_j)}{2m_j^2} + O(|m_j|^{-3}), \quad r \leq R_0, \\ &\rightarrow \frac{iy + Q/r}{|m_j|} + \frac{\text{sgn}(m_j)}{2m_j^2} + O(|m_j|^{-3}), \quad r > R_0, \end{aligned} \quad (41)$$

whereas the corresponding asymptotics of $\text{Tr}G_{m_j}^{(1)}(r; iy)$ reads

$$\text{Tr}G_{m_j}^{(1)}(r; iy) \rightarrow \begin{cases} V_0 \frac{1}{|m_j|} + O(|m_j|^{-3}), & r \leq R_0, \\ \frac{Q}{r} \frac{1}{|m_j|} + O(|m_j|^{-3}), & r > R_0. \end{cases} \quad (42)$$

Taking into account the definition of $\text{Tr}G_{|m_j|}(r, r; iy)$ (30), from (97) and (42) one obtains

$$\text{Re} \left[\text{Tr}G_{|m_j|}(r, r; iy) - 2 \text{Tr}G_{m_j}^{(1)}(r; iy) \right] = O(|m_j|^{-3}), \quad |m_j| \rightarrow \infty. \quad (43)$$

Proceeding further, let us note that the discrete levels should rise up with increasing $|m_j|$. Therefore for any given Q the additional contribution from negative discrete levels to $\rho_{VP}(r)$ disappears in the expressions (31) and (36) for $|m_j| \rightarrow \infty$. Since the integral over dy in (36) converges uniformly (see [29], App.C), there follows from (97) that $\rho_{VP,|m_j|}^{(3+)}(r)$ for $|m_j| \rightarrow \infty$ behaves as $O(|m_j|^{-3})$. So the partial series in m_j converges and the renormalized induced density $\rho_{VP}^{ren}(r)$ (39) is finite everywhere up to logarithmic singularities at $r = R_0$ due to the contribution from $\rho_{VP}^{(1)}(r)$.

Fig.2(a) shows the renormalized induced density $\rho_{VP}^{ren}(r)$ (39) for the unscreened ($R_1 \rightarrow \infty$) external potential (1) in the case $\alpha = 0.4$, $R_0 = 1/15$, first in the purely perturbative regime for $Z = 0.5$, thereupon for $Z = 2.37$, when the first $Z_{cr,1} \simeq 2.373$ isn't reached yet, for $Z = 2.38$, when the first discrete level has just dived into the lower continuum, thereon for $Z = 3.05$, when the second $Z_{cr,2} \simeq 3.056$ is not reached yet, and, finally, for $Z = 3.06$, i.e. just after diving of the second discrete level into the lower continuum. The critical charges are found from the transcendental equation, which is the consequence of matching conditions for $\psi_{m_j}^{in}(r)$ and $\psi_{m_j}^{out}(r)$ at $r = R_0$ for $\epsilon = -1$:

$$\begin{aligned} I_{|m_j-1/2|} \left(\sqrt{1 - (V_0 - 1)^2 R_0} \right) \left[K_{2i|\varkappa|-1} \left(\sqrt{8QR_0} \right) + K_{2i|\varkappa|+1} \left(\sqrt{8QR_0} \right) + \right. \\ \left. + \sqrt{\frac{2}{QR_0}} m_j K_{2i|\varkappa|} \left(\sqrt{8QR_0} \right) \right] + \sqrt{2(2 - V_0)} I_{|m_j+1/2|} \left(\sqrt{1 - (V_0 - 1)^2 R_0} \right) K_{2i|\varkappa|} \left(\sqrt{8QR_0} \right) = 0, \end{aligned} \quad (44)$$

In (44) $K_p(z)$ is the MacDonald function, which appears in the solutions of the system (19) in the limit $\epsilon \rightarrow -1$, while $|\varkappa| = \sqrt{Q^2 - m_j^2}$.

The direct numerical integration confirms that the total induced charge for $Z = 0.5$, 2.37 equals to zero, for $Z = 2.38, 3.05$ equals to $(-2|e|)$, while for $Z = 3.06$ equals to $(-4|e|)$. Fig.2(b) displays the logarithmic singularity in $\rho_{VP}^{ren}(r)$ at $r = R_0$, which originates from $\rho_{VP}^{(1)}(r)$. On the contrary, the induced density $\rho_{VP}^{(3+)}(r) = \sum_{m_j} \rho_{VP,|m_j|}^{(3+)}(r)$ is a continuous function, which is shown in Fig.2(c). Fig.2(d) displays the weighted sign-alternating density $r \times \rho_{VP}^{(3+)}(r)$ on a sufficiently large interval of variation of the radial variable for $Z = 2.37$, which confirms that the total induced charge in the subcritical region should vanish. Note also that in the overcritical region the changes of $\rho_{VP}^{ren}(r)$ with increasing Z proceed not only in a step-like manner due to the formation of vacuum shells from the discrete levels diving into the lower continuum according to (40) (which

is sometimes called a "real" polarization), but also via permanent deformations in the density of states in both continua and evolution of the discrete levels with increasing Z (known as a "virtual" one). For other values of α and R_0 similar graphs don't change qualitatively.

Thus, the correct approach to calculation of $\rho_{VP}^{ren}(r)$ for all the regions for Z should be based on the expressions (36) and (39) with subsequent verification of the expected integer value of the total induced charge via direct integration of $\rho_{VP}^{ren}(r)$.

4. INDUCED CHARGE DENSITY FOR THE SCREENED COULOMB ASYMPTOTICS

The changes start already in PT directly from the Uehling potential. Namely, the expression (7) for

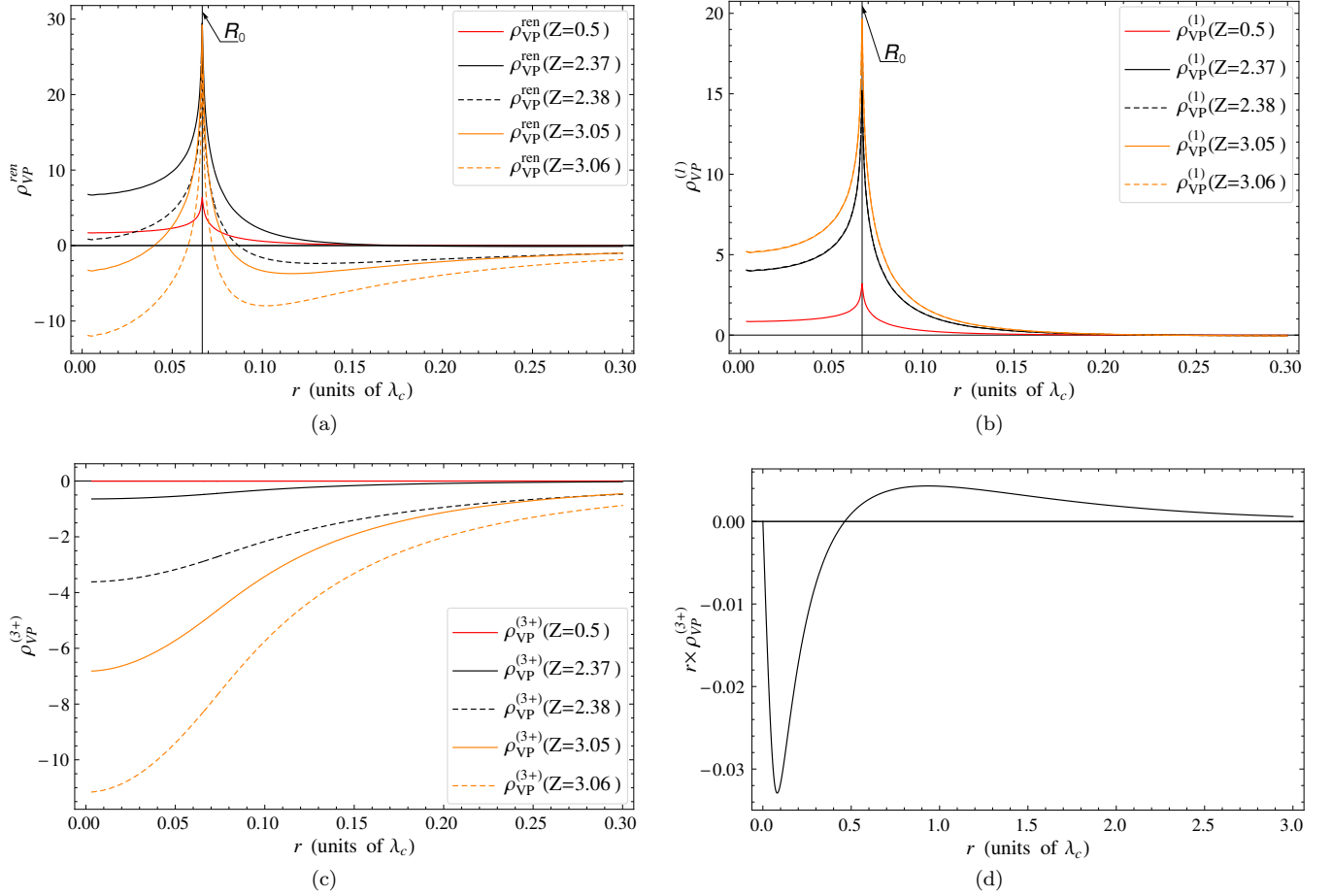


FIG. 2: (Color online) (a) $\rho_{VP}^{ren}(r)$, (b) $\rho_{VP}^{(1)}(r)$, (c) $\rho_{VP}^{(3+)}(r)$, $\alpha = 0.4, R_0 = 1/15$ and $Z = 0.5, 2.37, 2.38, 3.05, 3.06$, (d) $r \times \rho_{VP}^{(3+)}(r)$ on a more large interval of variation of the radial variable for $Z = 2.37$.

$A_{VP,0}^{(1)}(r)$ acquires the following additive term

$$\begin{aligned} \Delta A_{VP,0}^{(1)}(r) = & \frac{Z\alpha|e|}{4} \int_0^\infty dq \frac{J_0(qr)}{q} \left[\frac{2}{q} + \left(1 - \frac{4}{q^2}\right) \times \right. \\ & \left. \times \arctan\left(\frac{q}{2}\right) \right] \times (2[qR_1 J_0(qR_1) - 1] - \\ & - \pi q R_1 [J_0(qR_1) \mathbf{H}_1(qR_1) - J_1(qR_1) \mathbf{H}_0(qR_1)]) , \quad (45) \end{aligned}$$

which yields the corresponding contribution to the induced density

$$\begin{aligned} \Delta \rho_{VP}^{(1)}(r) = & -\frac{Z\alpha|e|}{16\pi} \Delta_2 \left(\int_0^\infty dq \frac{J_0(qr)}{q} \left[\frac{2}{q} + \left(1 - \frac{4}{q^2}\right) \times \right. \right. \\ & \left. \left. \times \arctan\left(\frac{q}{2}\right) \right] \times (2[qR_1 J_0(qR_1) - 1] - \right. \\ & \left. \left. - \pi q R_1 [J_0(qR_1) \mathbf{H}_1(qR_1) - J_1(qR_1) \mathbf{H}_0(qR_1)]) \right) \right) . \quad (46) \end{aligned}$$

Now in (46) it is not allowed to exchange the integration over dq and the Laplace operator, since in contrast to the

unscreened case the leading term of the integrand in (46) behaves for $q \rightarrow \infty$ as

$$-\frac{\cos(q(r+R_1)) + \sin(q(r-R_1))}{\sqrt{rR_1} q^2} , \quad (47)$$

which after the action of Δ_2 gives

$$\frac{\cos(q(r+R_1)) + \sin(q(r-R_1))}{\sqrt{rR_1}} + O(1/q) . \quad (48)$$

Such behavior of the asymptotics of the integrand for $\Delta \rho_{VP}^{(1)}(r)$ means that the induced density should reveal an even more strong singularity for $r \rightarrow R_1$, than for $r \rightarrow R_0$, namely

$$\begin{aligned} \Delta \rho_{VP}^{(1)}(r) \rightarrow & -\frac{Z\alpha|e|}{8\pi} \left(\frac{1}{2R_1(r-R_1)} + \right. \\ & \left. + \frac{1}{4R_1^2} \ln|R_1-r| + O(1) \right) , \quad r \rightarrow R_1 . \quad (49) \end{aligned}$$

Actually, the difference between the logarithmic singularity at $r = R_0$ and the power-like at $r = R_1$ in the induced density reflects the difference in behavior of the

external potential (1) at these points. A more detailed analysis of the structure of singularities in $\Delta\rho_{VP}^{(1)}(r)$ at $r = R_1$ is presented in [38].

It should be pointed out that for a slightly modified cutoff, which preserves the continuity of the potential at $r = R_1$, the singularity in $\rho_{VP}^{(1)}(r)$ at $r = R_1$ remains a logarithmic one, as for $r = R_0$. However, for the induced charge and density the discontinuity in the external potential (1) at $r = R_1$ doesn't pose any principal problems, in particular, $Q_{VP}^{(1)}$ remains zero. So we'll deal here with this type of screening, since (1) looks more physical and transparent. At the same time, the perturbative one-loop vacuum polarization energy turns out to be divergent due to this discontinuity, and so calculation of the Casimir (vacuum) energy in this case requires to consider a more soft type of screening (see, e.g., refs.[38, 39]).

Screening (1) yields the next changes in the structure of solutions of the radial DC problem (19). For $r \leq R_0$

the fundamental pair of solutions (20) remains the same, the fundamental pair (22) is now valid on the interval $R_0 < r < R_1$, while for the remaining part of the half-axis $r \geq R_1$ the independent solutions of (19) should be chosen as

$$\begin{aligned} \text{for } \psi_1(r) : \quad \mathcal{I}_1^0(r) &= \gamma I_{|m_j-1/2|}(\gamma r) , \\ \mathcal{K}_1^0(r) &= -\gamma K_{|m_j-1/2|}(\gamma r) ; \end{aligned} \quad (50)$$

$$\begin{aligned} \text{for } \psi_2(r) : \quad \mathcal{I}_2^0(r) &= (1 - \epsilon) I_{|m_j+1/2|}(\gamma r) , \\ \mathcal{K}_2^0(r) &= (1 - \epsilon) K_{|m_j+1/2|}(\gamma r) , \end{aligned} \quad (51)$$

where $\gamma = \sqrt{1 - \epsilon^2}$.

As a result, the expression for $\text{Tr}G_{m_j}$ in the screened case takes the form

$$\begin{aligned} \text{Tr}G_{m_j}(r, r; \epsilon) = & \\ \left\{ \begin{array}{ll} \frac{1}{[\mathcal{I}, \mathcal{K}]} \left(\mathcal{I}_1 \mathcal{K}_1 + \mathcal{I}_2 \mathcal{K}_2 + \frac{[\mathcal{K}^0, \mathcal{M}]_{R_1} [\mathcal{W}, \mathcal{K}]_{R_0} + [\mathcal{W}, \mathcal{K}^0]_{R_1} [\mathcal{M}, \mathcal{K}]_{R_0}}{[\mathcal{K}^0, \mathcal{M}]_{R_1} [\mathcal{I}, \mathcal{W}]_{R_0} + [\mathcal{W}, \mathcal{K}^0]_{R_1} [\mathcal{I}, \mathcal{M}]_{R_0}} (\mathcal{I}_1^2 + \mathcal{I}_2^2) \right), & r \leq R_0 , \\ \frac{1}{[\mathcal{M}, \mathcal{W}]} \left(\frac{[\mathcal{K}^0, \mathcal{M}]_{R_1} [\mathcal{W}, \mathcal{I}]_{R_0} + [\mathcal{W}, \mathcal{K}^0]_{R_1} [\mathcal{I}, \mathcal{M}]_{R_0}}{[\mathcal{K}^0, \mathcal{M}]_{R_1} [\mathcal{W}, \mathcal{I}]_{R_0} - [\mathcal{W}, \mathcal{K}^0]_{R_1} [\mathcal{I}, \mathcal{M}]_{R_0}} (\mathcal{M}_1 \mathcal{W}_1 + \mathcal{M}_2 \mathcal{W}_2) + \right. & \\ \left. \frac{[\mathcal{K}^0, \mathcal{M}]_{R_1} [\mathcal{I}, \mathcal{M}]_{R_0} (\mathcal{W}_1^2 + \mathcal{W}_2^2) + [\mathcal{W}, \mathcal{K}^0]_{R_1} [\mathcal{W}, \mathcal{I}]_{R_0} (\mathcal{M}_1^2 + \mathcal{M}_2^2)}{[\mathcal{K}^0, \mathcal{M}]_{R_1} [\mathcal{W}, \mathcal{I}]_{R_0} - [\mathcal{W}, \mathcal{K}^0]_{R_1} [\mathcal{I}, \mathcal{M}]_{R_0}} \right), & R_0 < r < R_1 , \\ \frac{1}{[\mathcal{I}^0, \mathcal{K}^0]} \left(\mathcal{I}_1^0 \mathcal{K}_1^0 + \mathcal{I}_2^0 \mathcal{K}_2^0 + \frac{[\mathcal{I}^0, \mathcal{W}]_{R_1} [\mathcal{I}, \mathcal{M}]_{R_0} + [\mathcal{I}^0, \mathcal{M}]_{R_1} [\mathcal{W}, \mathcal{I}]_{R_0}}{[\mathcal{W}, \mathcal{K}^0]_{R_1} [\mathcal{I}, \mathcal{M}]_{R_0} + [\mathcal{M}, \mathcal{K}^0]_{R_1} [\mathcal{W}, \mathcal{I}]_{R_0}} ((\mathcal{K}_1^0)^2 + (\mathcal{K}_2^0)^2) \right), & r \geq R_1 , \end{array} \right. & (52) \end{aligned}$$

where in addition to (25) one has

$$[\mathcal{I}^0, \mathcal{K}^0] = \epsilon - 1 , \quad (53)$$

while the Wronskian (18), which enters into the expression for $\text{Tr}G_{m_j}$ (17), equals now to

$$J_{m_j}(\epsilon) = \frac{[\mathcal{K}^0, \mathcal{M}]_{R_1} [\mathcal{I}, \mathcal{W}]_{R_0} + [\mathcal{W}, \mathcal{K}^0]_{R_1} [\mathcal{I}, \mathcal{M}]_{R_0}}{[\mathcal{M}, \mathcal{W}]} . \quad (54)$$

The asymptotics of $\text{Tr}G_{m_j}(r, r; \epsilon)$ on the arcs of large circle (Fig.1) for $r \leq R_0$ and $R_0 < r < R_1$ coincide with those in the problem without screening (27) and (28), since the terms in $\text{Tr}G_{m_j}$, depending on R_1 , give only an exponentially decreasing contribution. For $r \geq R_1$ the asymptotics of $\text{Tr}G_{m_j}(r, r; \epsilon)$ takes the form: on the arcs $C_1(R)$ and $C_2(R)$ in the upper half-plane,

where $|\epsilon| \rightarrow \infty$, $0 < \text{Arg } \epsilon < \pi$,

$$\begin{aligned} \text{Tr}G_{m_j}(r, r; \epsilon) \rightarrow & \\ \frac{i}{r} + \frac{i}{2r\epsilon^2} \left(\frac{m_j^2}{r^2} + 1 \right) - \frac{im_j}{2r^3\epsilon^3} + O(|\epsilon|^{-4}) , & r \geq R_1 ; \end{aligned} \quad (55)$$

on the arcs of large circle in the lower half-plane $C_3(R)$ and $C_4(R)$, where $|\epsilon| \rightarrow \infty$, $-\pi < \text{Arg } \epsilon < 0$,

$$\begin{aligned} \text{Tr}G_{m_j}(r, r; \epsilon) \rightarrow & \\ -\frac{i}{r} - \frac{i}{2r\epsilon^2} \left(\frac{m_j^2}{r^2} + 1 \right) + \frac{im_j}{2r^3\epsilon^3} + O(|\epsilon|^{-4}) , & r \geq R_1 . \end{aligned} \quad (56)$$

Again, there follows from the asymptotics of $\text{Tr}G_{m_j}(r, r; \epsilon)$ on the arcs of the large circle that the integration along the contours $P(R)$ and $E(R)$ in (15) can be reduced to the imaginary axis, whence one finds the same final expression for the vacuum density as in the

unscreened case (29)-(31) with the same properties (32)-(34).

However, the asymptotics of $\text{Tr}G_{m_j}(r, r; \epsilon)$ for $r \rightarrow \infty$ undergoes significant changes, caused by the different structure (50),(51) of solutions of the system (19) for $r \geq R_1$, namely

$$\text{Tr}G_{m_j}(r, r; iy) \rightarrow \frac{iy}{\sqrt{1+y^2}} \frac{1}{r} + \frac{m_j(1-im_jy)}{2(1+y^2)^{3/2}} \frac{1}{r^3} + O\left(\frac{1}{r^5}\right), \quad r \rightarrow \infty. \quad (57)$$

There follows from (57) that in the case of finite R_1 for any m_j the total induced charge is finite from the outset. Nevertheless, the induced density requires renormalization, since the non-renormalized total induced charge doesn't vanish in the subcritical region. For these purposes we define once more the component $\rho_{VP,|m_j|}^{(3+)}(r)$ by the same expression (36), where $\text{Tr}G_{m_j}^{(1)}(r; iy)$ should now be replaced by:

for $r \leq R_0$

$$\begin{aligned} \text{Tr}G_{m_j}^{(1)}(r; iy) = & \frac{Q}{(iy-1)^2} \left[\left(\tilde{\gamma}^2 K_{|m_j-1/2|}^2(\tilde{\gamma}r) + (1-iy)^2 K_{|m_j+1/2|}^2(\tilde{\gamma}r) \right) \int_0^r dr' \frac{r'}{R_0} \left(\tilde{\gamma}^2 I_{|m_j-1/2|}^2(\tilde{\gamma}r') + \right. \right. \\ & \left. \left. + (1-iy)^2 I_{|m_j+1/2|}^2(\tilde{\gamma}r') \right) + \left(\tilde{\gamma}^2 I_{|m_j-1/2|}^2(\tilde{\gamma}r) + (1-iy)^2 I_{|m_j+1/2|}^2(\tilde{\gamma}r) \right) \times \right. \\ & \left. \times \left\{ \int_r^{R_0} dr' \frac{r'}{R_0} \left(\tilde{\gamma}^2 K_{|m_j-1/2|}^2(\tilde{\gamma}r') + (1-iy)^2 K_{|m_j+1/2|}^2(\tilde{\gamma}r') \right) + \right. \right. \\ & \left. \left. + \int_{R_0}^{R_1} dr' \left(\tilde{\gamma}^2 K_{|m_j-1/2|}^2(\tilde{\gamma}r') + (1-iy)^2 K_{|m_j+1/2|}^2(\tilde{\gamma}r') \right) \right\} \right], \quad (58) \end{aligned}$$

for $R_0 < r < R_1$

$$\begin{aligned} \text{Tr}G_{m_j}^{(1)}(r; iy) = & \frac{Q}{(iy-1)^2} \left[\left(\tilde{\gamma}^2 K_{|m_j-1/2|}^2(\tilde{\gamma}r) + (1-iy)^2 K_{|m_j+1/2|}^2(\tilde{\gamma}r) \right) \left\{ \int_0^{R_0} dr' \frac{r'}{R_0} \left(\tilde{\gamma}^2 I_{|m_j-1/2|}^2(\tilde{\gamma}r') + \right. \right. \right. \\ & \left. \left. + (1-iy)^2 I_{|m_j+1/2|}^2(\tilde{\gamma}r') \right) + \int_{R_0}^r dr' \left(\tilde{\gamma}^2 I_{|m_j-1/2|}^2(\tilde{\gamma}r') + (1-iy)^2 I_{|m_j+1/2|}^2(\tilde{\gamma}r') \right) \right\} + \\ & \left. + \left(\tilde{\gamma}^2 I_{|m_j-1/2|}^2(\tilde{\gamma}r) + (1-iy)^2 I_{|m_j+1/2|}^2(\tilde{\gamma}r) \right) \int_r^{R_1} dr' \left(\tilde{\gamma}^2 K_{|m_j-1/2|}^2(\tilde{\gamma}r') + \right. \right. \\ & \left. \left. + (1-iy)^2 K_{|m_j+1/2|}^2(\tilde{\gamma}r') \right) \right], \quad (59) \end{aligned}$$

for $r \geq R_1$

$$\begin{aligned} \text{Tr}G_{m_j}^{(1)}(r; iy) = & \frac{Q}{(iy-1)^2} \left[\left(\tilde{\gamma}^2 K_{|m_j-1/2|}^2(\tilde{\gamma}r) + (1-iy)^2 K_{|m_j+1/2|}^2(\tilde{\gamma}r) \right) \left\{ \int_0^{R_0} dr' \frac{r'}{R_0} \left(\tilde{\gamma}^2 I_{|m_j-1/2|}^2(\tilde{\gamma}r') + \right. \right. \right. \\ & \left. \left. + (1-iy)^2 I_{|m_j+1/2|}^2(\tilde{\gamma}r') \right) + \int_{R_0}^{R_1} dr' \left(\tilde{\gamma}^2 I_{|m_j-1/2|}^2(\tilde{\gamma}r') + (1-iy)^2 I_{|m_j+1/2|}^2(\tilde{\gamma}r') \right) \right\} \right], \quad (60) \end{aligned}$$

where $\tilde{\gamma} = \sqrt{1+y^2}$, and introduce the renormalized $\rho_{VP}^{ren}(r)$ via expression

$$\rho_{VP}^{ren}(r) = 2 \left[\rho_{VP}^{(1)}(r) + \Delta\rho_{VP}^{(1)}(r) + \sum_{m_j=1/2, 3/2, \dots} \rho_{VP,|m_j|}^{(3+)}(r) \right], \quad (61)$$

with $\rho_{VP}^{(1)}(r)$ being the perturbative induced density (10) for the unscreened case, while $\Delta\rho_{VP}^{(1)}(r)$ is the additional

contribution (46), caused by finite R_1 .

Qualitatively, the behavior of the renormalized induced density (61) looks like in the unscreened case ($R_1 \rightarrow \infty$): for $Z < Z_{cr,1}$ the total induced charge vanishes exactly, each discrete level $\psi_{n,m_j}(r)$ by diving into the lower continuum yields the change in the induced density described by (40), while the total induced charge loses an amount equal to $(-2|e|)$. To demonstrate the correspondence between the screened and unscreened cases, in Figs.3a-d there are shown the components of the induced density $\rho_{VP,|m_j|}^{(3+)}(r)$ for the case $\alpha = 0.4$, $R_0 = 1/15$, $|m_j| = 3/2$ and $R_1 = \infty, 10 R_0, 5 R_0, 2 R_0$, correspondingly. Each plot contains the induced density before and just after diving of the first discrete level into the lower continuum. Moreover, from Figs.3a-d it is clearly seen that for decreasing R_1 the components of the induced density $\rho_{VP,|m_j|}^{(3+)}(r)$ localize in the region $r \sim R_0$ due to contraction of the Coulomb well.

5. PECULIAR EFFECTS IN THE SCREENED TWO-DIMENSIONAL CASE

In the screened two-dimensional case the behavior of levels at thresholds of both continua reveals some peculiar features, which are quite different from the unscreened one and absent in one- or three-dimensional DC systems. As in the previous Section, we'll consider them here for the screened potential (1).

It would be instructive to start directly with the DC spectral problem (19) at the lower threshold. For $\epsilon = -1$ the system (19) takes the form

$$\begin{cases} \frac{d}{dr}\psi_1(r) + \frac{1/2 - m_j}{r}\psi_1(r) = -V(r)\psi_2(r) , \\ \frac{d}{dr}\psi_2(r) + \frac{1/2 + m_j}{r}\psi_2(r) = (2 + V(r))\psi_1(r) . \end{cases} \quad (62)$$

For $r \leq R_0$ the solutions of (62) can be represented as

$$\begin{aligned} \psi_1(r) &= \sqrt{V_0} I_{|m_j-1/2|} \left(\sqrt{V_0(2-V_0)} r \right) , \\ \psi_2(r) &= \sqrt{2-V_0} I_{|m_j+1/2|} \left(\sqrt{V_0(2-V_0)} r \right) , \end{aligned} \quad (63)$$

while for $R_0 < r < R_1$ they should be written as follows

$$\begin{aligned} \psi_1(r) &= \sqrt{\frac{2Q}{r}} \left(\lambda K_{2i|z|} \left(\sqrt{8Qr} \right) + I_{2i|z|} \left(\sqrt{8Qr} \right) \right) , \\ \psi_2(r) &= 2I_{1+2i|z|} \left(\sqrt{8Qr} \right) + \\ &+ (i|z| - m_j) \sqrt{\frac{2}{Qr}} I_{2i|z|} \left(\sqrt{8Qr} \right) - \\ &- \lambda \left(2K_{1+2i|z|} \left(\sqrt{8Qr} \right) - \right. \\ &\left. - (i|z| - m_j) \sqrt{\frac{2}{Qr}} K_{2i|z|} \left(\sqrt{8Qr} \right) \right) . \end{aligned} \quad (64)$$

The coefficient λ is determined by matching the solutions (63) and (64) at $r = R_0$.

The new circumstance, which is specific to the screened two-dimensional case, is that for $r \geq R_1$ the solutions of (62) turn out to be the power-like ones, which degree separates the channels with $|m_j| = 1/2$, $m_j = -3/2$ and the others into two essentially different groups. Namely, for $m_j \geq 3/2$ and $m_j \leq -5/2$ the solutions of (62) in the region $r \geq R_1$ up to a common normalization factor take the form

$$\begin{aligned} m_j \geq 3/2 : \psi_1(r) &= 0, \psi_2(r) = r^{-(m_j+1/2)}, \\ m_j \leq -5/2 : \psi_1(r) &= r^{m_j-1/2}, \psi_2(r) = \frac{r^{m_j+1/2}}{m_j+1/2}, \end{aligned} \quad (65)$$

which leads to normalizable discrete levels at $\epsilon = -1$. For these channels the corresponding critical charges are found via matching at $r = R_1$, what gives

$$W_{1,m_j}^- = 0 \quad (66)$$

for $m_j \geq 3/2$ and

$$W_{2,|m_j|}^- = 0 , \quad (67)$$

for $m_j \leq -5/2$, where ($m_j > 0$)

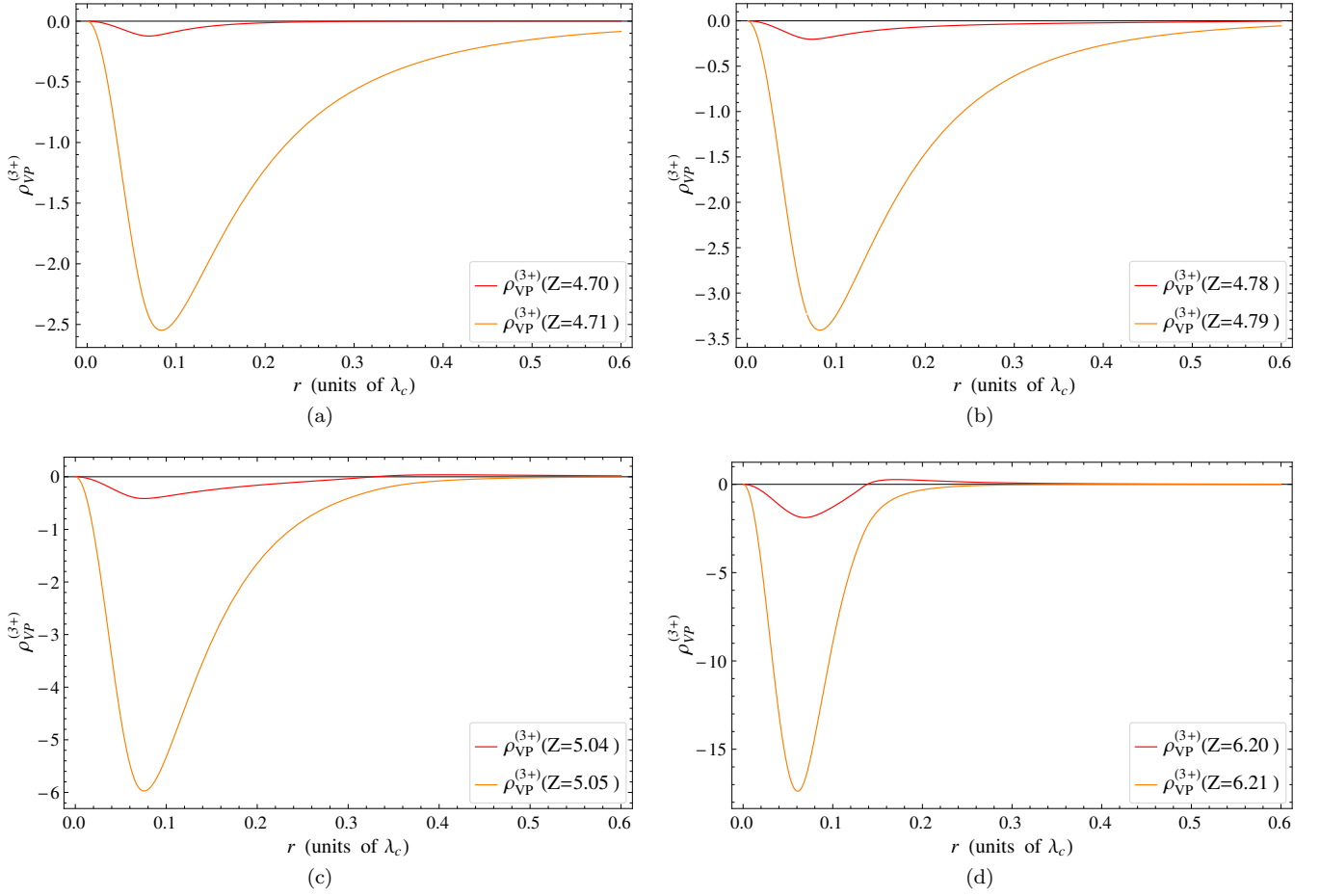


FIG. 3: (Color online) $\rho_{VP,3/2}^{(3+)}(r)$ for $\alpha = 0.4$, $R_0 = 1/15$ and (a) $R_1 \rightarrow \infty$, (b) $R_1 = 10R_0$, (c) $R_1 = 5R_0$, (d) $R_1 = 2R_0$.

$$\begin{aligned}
W_{1,m_j}^\mp &= K_{2i|\varkappa|} \left(\sqrt{\pm 8QR_1} \right) \times \\
&\times \left(I_{m_j-1/2}(\sqrt{\pm V_0(2 \mp V_0)} R_0) \left(2I_{1+2i|\varkappa|}(\sqrt{\pm 8QR_0}) \pm (i|\varkappa| - m_j) \sqrt{\frac{2}{\pm QR_0}} I_{2i|\varkappa|}(\sqrt{\pm 8QR_0}) \right) - \right. \\
&- \left. \sqrt{2(2 \mp V_0)} I_{m_j+1/2}(\sqrt{\pm V_0(2 \mp V_0)} R_0) I_{2i|\varkappa|}(\sqrt{\pm 8QR_0}) \right) + \\
&+ I_{2i|\varkappa|} \left(\sqrt{\pm 8QR_1} \right) \times \\
&\times \left(I_{m_j-1/2}(\sqrt{\pm V_0(2 \mp V_0)} R_0) \left(2K_{1+2i|\varkappa|}(\sqrt{\pm 8QR_0}) \mp (i|\varkappa| - m_j) \sqrt{\frac{2}{\pm QR_0}} K_{2i|\varkappa|}(\sqrt{\pm 8QR_0}) \right) + \right. \\
&+ \left. \sqrt{2(2 \mp V_0)} I_{m_j+1/2}(\sqrt{\pm V_0(2 \mp V_0)} R_0) K_{2i|\varkappa|}(\sqrt{\pm 8QR_0}) \right), \tag{68}
\end{aligned}$$

$$\begin{aligned}
W_{2,m_j}^{\mp} = & \left(\sqrt{\pm 2Q} K_{2i|z|} \left(\sqrt{\pm 8QR_1} \right) - \frac{m_j - 1/2}{\sqrt{R_1}} \left(2K_{1+2i|z|} \left(\sqrt{\pm 8QR_1} \right) \mp (i|z| + m_j) \sqrt{\frac{2}{\pm QR_1}} K_{2i|z|} \left(\sqrt{\pm 8QR_1} \right) \right) \right) \times \\
& \times \left(I_{m_j+1/2} \left(\sqrt{\pm V_0(2 \mp V_0)} R_0 \right) \left(2I_{1+2i|z|} \left(\sqrt{\pm 8QR_0} \right) \pm (i|z| + m_j) \sqrt{\frac{2}{\pm QR_0}} I_{2i|z|} \left(\sqrt{\pm 8QR_0} \right) \right) - \right. \\
& - \sqrt{2(2 \mp V_0)} I_{m_j-1/2} \left(\sqrt{\pm V_0(2 \mp V_0)} R_0 \right) I_{2i|z|} \left(\sqrt{\pm 8QR_0} \right) \left. \right) + \\
& + \left(\sqrt{\pm 2Q} I_{2i|z|} \left(\sqrt{\pm 8QR_1} \right) + \frac{m_j - 1/2}{\sqrt{R_1}} \left(2I_{1+2i|z|} \left(\sqrt{\pm 8QR_1} \right) \pm (i|z| + m_j) \sqrt{\frac{2}{\pm QR_1}} I_{2i|z|} \left(\sqrt{\pm 8QR_0} \right) \right) \right) \times \\
& \times \left(I_{m_j+1/2} \left(\sqrt{\pm V_0(2 \mp V_0)} R_0 \right) \left(2K_{1+2i|z|} \left(\sqrt{\pm 8QR_0} \right) \mp (i|z| + m_j) \sqrt{\frac{2}{\pm QR_0}} K_{2i|z|} \left(\sqrt{\pm 8QR_0} \right) \right) + \right. \\
& + \sqrt{2(2 \mp V_0)} I_{m_j-1/2} \left(\sqrt{\pm V_0(2 \mp V_0)} R_0 \right) K_{2i|z|} \left(\sqrt{\pm 8QR_0} \right) \left. \right). \tag{69}
\end{aligned}$$

At the same time, for $|m_j| = 1/2$ and $m_j = -3/2$ the system (62) doesn't possess normalizable solutions at the lower threshold, since for $r \geq R_1$ one finds

$$\begin{aligned}
m_j = 1/2 & : \psi_1(r) = 0, \quad \psi_2(r) = A/r, \\
m_j = -1/2 & : \psi_1(r) = 0, \quad \psi_2(r) = B, \\
m_j = -3/2 & : \psi_1(r) = C/r^2, \quad \psi_2(r) = -C/r. \tag{70}
\end{aligned}$$

Moreover, the solutions (70) cannot be interpreted as the scattering states at the lower threshold too, since in the latter case both components of the WF should demonstrate the behavior typical for the cylindrical waves, namely $\sim 1/\sqrt{r}$. Remarkably enough, such form of solutions (70) for $r > R_1$ is a specific feature of two spatial dimensions. In the one-dimensional case the corresponding solutions at both thresholds are the scattering states with vanishing wavenumber. In 3 spatial dimensions, on the contrary, at the lower threshold the electronic WF for any orbital number l contains only one

non-vanishing component, which behaves like $O(r^{-(l+2)})$ and so all the states belong to the discrete spectrum, whereas at the upper threshold the s -wave is the scattering state, while the others again belong to the discrete spectrum.

In Figs.4a,b there are shown the components $\psi_1(r)$ and $\psi_2(r)$ of the electronic WF, corresponding to levels with $m_j = \pm 1/2$, lying very close to the threshold, namely $\epsilon = -0.9999999999999999999999999999999762$ ($Z = 3.808194785685109813175$) for $m_j = 1/2$ and $\epsilon = -0.9999999999999999999999999999999773$ ($Z = 5.57$) for $m_j = -1/2$. Figs.4c,d represent $\psi_1(r)$ and $\psi_2(r)$ of levels with $m_j = \pm 3/2$ for $\epsilon = -0.999999113$ ($Z = 6.2059331$) and $\epsilon = -0.999999118$ ($Z = 6.38159669$), respectively.

Although in this case we deal with non-normalizable solutions, the equations for the corresponding critical charges can be also found via matching the solutions (64) and (70) at $r = R_1$, what gives:

for $m_j = 1/2$

$$\begin{aligned}
\text{Im} \left[\left(Q \sqrt{1 - \frac{2}{V_0}} J_{-2i|z|}(-2\sqrt{-2QR_0}) J_1(\sqrt{V_0(V_0 - 2)} R_0) + \right. \right. \\
\left. \left. + \left(\sqrt{-2QR_0} J_{1-2i|z|}(-2\sqrt{-2QR_0}) - (1/2 + i|z|) J_{-2i|z|}(-2\sqrt{-2QR_0}) \right) J_0(\sqrt{V_0(V_0 - 2)} R_0) \right) \times \right. \\
\left. \times J_{2i|z|}(2\sqrt{-2QR_1}) \right] = 0, \tag{71}
\end{aligned}$$

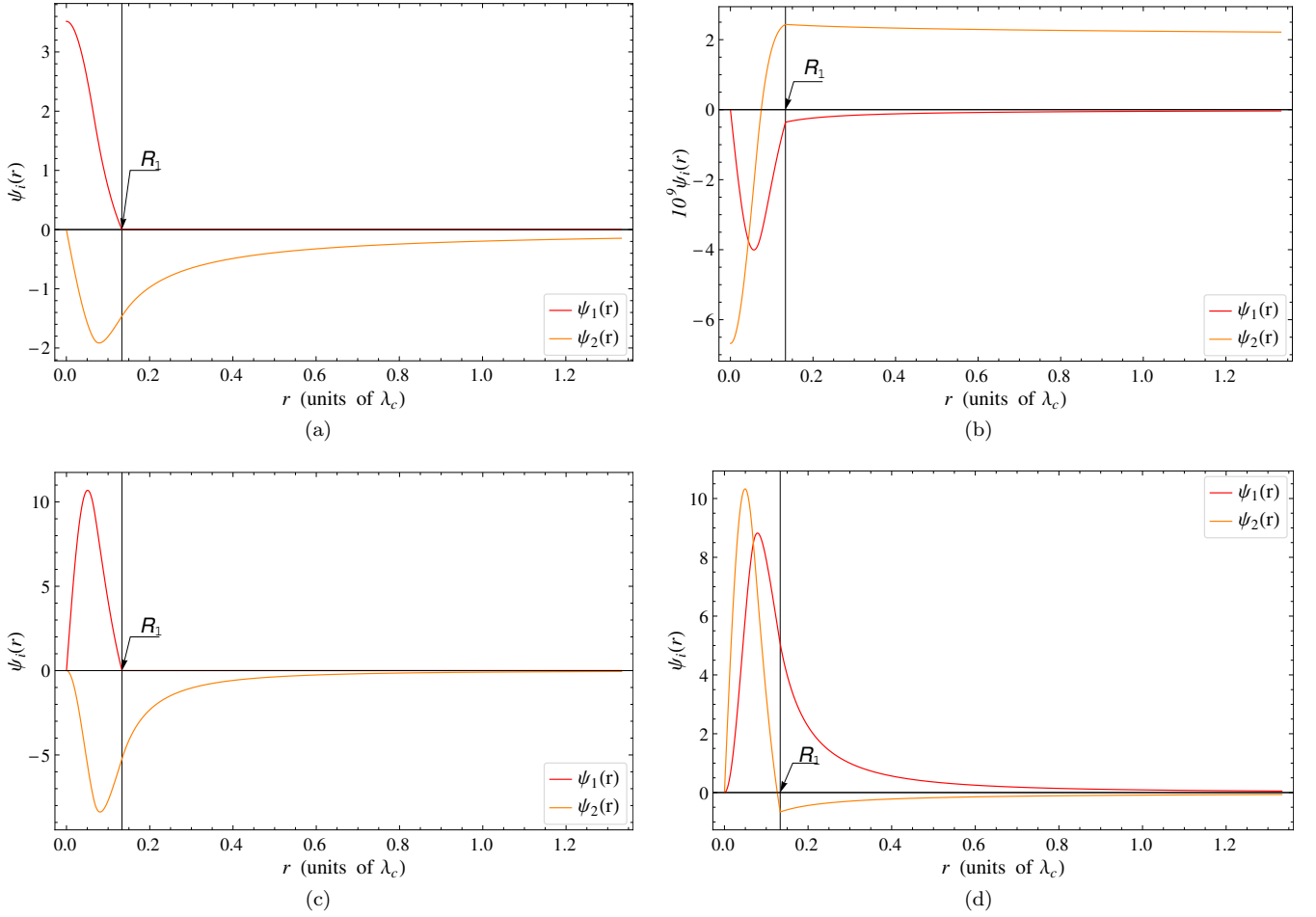


FIG. 4: (Color online) $\psi_1(r)$ and $\psi_2(r)$ for $\alpha = 0.4$, $R_0 = 1/15$, $R_1 = 2R_0$ and (a) $m_j = 1/2$, $Z = 3.808194785685109813175$, (b) $m_j = -1/2$, $Z = 5.57$, (c) $m_j = 3/2$, $Z = 6.2059331$, (d) $m_j = -3/2$, $Z = 6.38159669$.

for $m_j = -1/2$

$$\text{Im} \left[\left(Q \sqrt{1 - \frac{2}{V_0}} J_{-2i|\varkappa|}(-2\sqrt{-2QR_0}) J_1(\sqrt{V_0(V_0 - 2)} R_0) - \right. \right. \\ \left. \left. - \left(\sqrt{-2QR_0} J_{1-2i|\varkappa|}(-2\sqrt{-2QR_0}) + (1/2 - i|\varkappa|) J_{-2i|\varkappa|}(-2\sqrt{-2QR_0}) \right) J_1(\sqrt{V_0(V_0 - 2)} R_0) \right) \times \right. \\ \left. \times J_{2i|\varkappa|}(2\sqrt{-2QR_1}) \right] = 0, \quad (72)$$

and for $m_j = -3/2$

$$\text{Im} \left[\left(Q \sqrt{1 - \frac{2}{V_0}} J_{-2i|\varkappa|}(-2\sqrt{-2QR_0}) J_1(\sqrt{V_0(V_0 - 2)} R_0) - \right. \right. \\ \left. \left. - \left(\sqrt{-2QR_0} J_{1-2i|\varkappa|}(-2\sqrt{-2QR_0}) + (3/2 - i|\varkappa|) J_{-2i|\varkappa|}(-2\sqrt{-2QR_0}) \right) J_2(\sqrt{V_0(V_0 - 2)} R_0) \right) \times \right. \\ \left. \times \left((QR_1 + 3/2 + i|\varkappa|) J_{2i|\varkappa|}(2\sqrt{-2QR_1}) - \sqrt{-2QR_1} J_{1+2i|\varkappa|}(2\sqrt{-2QR_1}) \right) \right] = 0. \quad (73)$$

The validity of these equations can be easily verified by taking the limit $\epsilon \rightarrow -1$ in the equations for discrete levels

with $-1 < \epsilon < 1$ and $|m_j| < Q$ for the screened potential (1)

$$\begin{aligned} & \text{Im} \left[\left(K_{m_j+1/2}(\gamma R_1) ((m_j + Q/\gamma)\Phi(b, c, 2\gamma R_1) + b\Phi(b+1, c, 2\gamma R_1)) + \right. \right. \\ & \quad \left. \left. K_{m_j-1/2}(\gamma R_1) (-(m_j + Q/\gamma)\Phi(b, c, 2\gamma R_1) + b\Phi(b+1, c, 2\gamma R_1)) \right) \right. \\ & \quad \times \left(\sqrt{(\epsilon + V_0 + 1)(1 - \epsilon)} J_{m_j-1/2}(\zeta R_0) (-(Q/\gamma + m_j)\Phi^*(b, c, 2\gamma R_0) + b^* \Phi^*(b+1, c, 2\gamma R_0)) \right. \\ & \quad \left. \left. + \sqrt{(\epsilon + V_0 - 1)(1 + \epsilon)} J_{m_j+1/2}(\zeta R_0) ((Q/\gamma + m_j)\Phi^*(b, c, 2\gamma R_0) + b^* \Phi^*(b+1, c, 2\gamma R_0)) \right) \right] = 0. \quad (74) \end{aligned}$$

The mirror-symmetrical situation takes place now at the threshold of the upper continuum, since in the screened case the condensation of levels at $\epsilon \rightarrow 1$ disappears and the total number of discrete levels becomes finite. The whole difference is the change in signs of m_j . Namely, for $\epsilon = 1$ the system (19) takes the form

$$\begin{cases} \frac{d}{dr} \psi_1(r) + \frac{1/2 - m_j}{r} \psi_1(r) = (2 - V(r)) \psi_2(r), \\ \frac{d}{dr} \psi_2(r) + \frac{1/2 + m_j}{r} \psi_2(r) = V(r) \psi_1(r). \end{cases} \quad (75)$$

For $r \leq R_0$ the solutions of (75) are chosen as

$$\begin{aligned} \psi_1(r) &= \sqrt{V_0 + 2} I_{|m_j-1/2|} \left(\sqrt{-V_0(2 + V_0)} r \right), \\ \psi_2(r) &= \sqrt{V_0} I_{|m_j+1/2|} \left(\sqrt{-V_0(2 + V_0)} r \right), \end{aligned} \quad (76)$$

while for $R_0 < r < R_1$ they should be written as follows

$$\begin{aligned} \psi_1(r) &= 2I_{1+2i|\varkappa|} \left(\sqrt{-8Qr} \right) + \\ &+ (i|\varkappa| - m_j) \sqrt{\frac{2}{-Qr}} I_{2i|\varkappa|} \left(\sqrt{-8Qr} \right) - \\ &- \lambda \left(2K_{1+2i|\varkappa|} \left(\sqrt{-8Qr} \right) - \right. \\ &\left. - (i|\varkappa| - m_j) \sqrt{\frac{2}{-Qr}} K_{2i|\varkappa|} \left(\sqrt{-8Qr} \right) \right), \\ \psi_2(r) &= \sqrt{\frac{-2Q}{r}} \left(\lambda K_{2i|\varkappa|} \left(\sqrt{-8Qr} \right) + I_{2i|\varkappa|} \left(\sqrt{-8Qr} \right) \right), \end{aligned} \quad (77)$$

where the coefficient λ quite similar to the lower threshold is found via matching of solutions (76) and (77) at the point $r = R_0$.

Again, for $r \geq R_1$ the solutions of (75) turn out to be the power-like ones, whose degree separates now the channels with $|m_j| = 1/2$, $m_j = 3/2$ and the others into

two essentially different groups. Namely, for $m_j \geq 5/2$ and $m_j \leq -3/2$ for the solutions of (75) in the region $r \geq R_1$ up to a common normalization factor one finds

$$\begin{aligned} m_j \geq 5/2 : \psi_1(r) &= \frac{r^{1/2-m_j}}{1/2 - m_j}, \quad \psi_2(r) = r^{-m_j-1/2}, \\ m_j \leq -3/2 : \psi_1(r) &= r^{m_j-1/2}, \quad \psi_2(r) = 0. \end{aligned} \quad (78)$$

These solutions give rise to normalizable discrete levels at $\epsilon = 1$. The corresponding ‘‘upper critical’’ charges, when the virtual levels, descending to the threshold of the upper continuum from above, transform into the real ones, can be found from equations, which are derived by matching the solutions of (75) at the point $r = R_1$, namely

$$W_{2,m_j}^+ = 0 \quad (79)$$

for $m_j \geq 5/2$ and

$$W_{1,|m_j|}^+ = 0 \quad (80)$$

for $m_j \leq -3/2$.

For $|m_j| = 1/2$ and $m_j = 3/2$ the system (75) doesn't possess normalizable solutions at the upper threshold, which could be classified either as discrete levels or as the scattering states, since for $r \geq R_1$ the latter take the form

$$\begin{aligned} m_j = 1/2 : \psi_1(r) &= B, \quad \psi_2(r) = 0, \\ m_j = -1/2 : \psi_1(r) &= A/r, \quad \psi_2(r) = 0, \\ m_j = 3/2 : \psi_1(r) &= -C/r, \quad \psi_2(r) = C/r^2. \end{aligned} \quad (81)$$

The corresponding equations, defining the upper critical charges, are found now by the same procedure as for the lower ones and read:

for $m_j = 1/2$

$$\begin{aligned} \text{Im} \left[\left(Q \sqrt{1 + \frac{2}{V_0}} J_{-2i|\varkappa|}(2\sqrt{2QR_0}) J_0(\sqrt{V_0(V_0+2)} R_0) + \right. \right. \\ \left. \left. + \left(\sqrt{2QR_0} J_{1-2i|\varkappa|}(2\sqrt{2QR_0}) - (1/2 - i|\varkappa|) J_{-2i|\varkappa|}(2\sqrt{2QR_0}) \right) J_1(\sqrt{V_0(V_0+2)} R_0) \right) J_{2i|\varkappa|}(2\sqrt{2QR_1}) \right] = 0, \end{aligned} \quad (82)$$

for $m_j = -1/2$

$$\begin{aligned} \text{Im} \left[\left(-Q \sqrt{1 + \frac{2}{V_0}} J_{-2i|\varkappa|}(2\sqrt{2QR_0}) J_1(\sqrt{V_0(V_0+2)} R_0) + \right. \right. \\ \left. \left. + \left(\sqrt{2QR_0} J_{1-2i|\varkappa|}(2\sqrt{2QR_0}) + (1/2 + i|\varkappa|) J_{-2i|\varkappa|}(2\sqrt{2QR_0}) \right) J_0(\sqrt{V_0(V_0+2)} R_0) \right) J_{2i|\varkappa|}(2\sqrt{2QR_1}) \right] = 0, \end{aligned} \quad (83)$$

while for $m_j = 3/2$

$$\begin{aligned} \text{Im} \left[\left(Q \sqrt{1 + \frac{2}{V_0}} J_{-2i|\varkappa|}(2\sqrt{2QR_0}) J_1(\sqrt{V_0(V_0+2)} R_0) + \right. \right. \\ \left. \left. + \left(\sqrt{2QR_0} J_{1-2i|\varkappa|}(2\sqrt{2QR_0}) - (3/2 - i|\varkappa|) J_{-2i|\varkappa|}(2\sqrt{2QR_0}) \right) J_2(\sqrt{V_0(V_0+2)} R_0) \right) \times \right. \\ \left. \times \left((QR_1 - 3/2 - i|\varkappa|) J_{2i|\varkappa|}(2\sqrt{2QR_1}) + \sqrt{2QR_1} J_{1+2i|\varkappa|}(2\sqrt{2QR_1}) \right) \right] = 0. \end{aligned} \quad (84)$$

The peculiar feature of the channel $|m_j| = 1/2$ is a substantial difference in behavior of discrete levels in this channel by approaching both thresholds, not only between this channel and the others, but also between $m_j = 1/2$ and $m_j = -1/2$. Moreover, the last difference turns out to be the most impressive. Figs.5a,b represent the evolution of existing discrete levels on the interval $0 < Z < 10$ by growing Z for $\alpha = 0.4$, $R_0 = 1/15$, $R_1 = 2R_0$ and $|m_j| = 1/2, 3/2$. The vertical dashed lines denote the positions of the lower critical charges, when the levels approach the lower threshold, while the dotted ones — the upper ones, i.e. the moments of transformation of virtual levels into the real ones at the upper threshold. Fig.5a corresponds to $|m_j| = 1/2$, while Fig.5b to $|m_j| = 3/2$.

Such impressive difference in behavior of levels with $m_j = \pm 1/2$ near the thresholds can be well understood with account of expansion of corresponding equations for discrete levels with $-1 < \epsilon < 1$ and $|m_j| < Q$ (74) for $\epsilon \rightarrow \pm 1$. Namely, for $\epsilon \rightarrow -1$ the expansion of the corresponding equation for the levels with $m_j = 1/2$ gives

$$A_0 (Q/\gamma^2 + m_j/\gamma) + C_0 \ln \gamma + D_0 = 0, \quad (85)$$

with $\gamma = \sqrt{1 - \epsilon^2}$, while the coefficients A_0, B_0, C_0, D_0 are determined by the following expressions

$$A_0(Q, R_1) = \frac{\sqrt{8V_0}}{R_1} \text{Im} \left[B_0(Q) J_{-2i|\varkappa|}(-2\sqrt{-2QR_1}) \right], \quad (86)$$

$$\begin{aligned} B_0(Q) = Q \sqrt{1 - \frac{2}{V_0}} J_{2i|\varkappa|}(2\sqrt{-2QR_0}) J_1(R_0 \sqrt{(V_0 - 2)V_0}) - \\ - \left(\sqrt{-2QR_0} J_{1+2i|\varkappa|}(2\sqrt{-2QR_0}) + (1/2 - i|\varkappa|) J_{2i|\varkappa|}(2\sqrt{-2QR_0}) \right) J_0(R_0 \sqrt{(V_0 - 2)V_0}), \end{aligned} \quad (87)$$

$$\begin{aligned} C_0(Q, R_1) = \text{Im} \left[B_0(Q) (QR_1 J_{-2i|\varkappa|}(-2\sqrt{-2QR_1}) - \right. \\ \left. - (\sqrt{-2QR_1} J_{1-2i|\varkappa|}(-2\sqrt{-2QR_1}) - (1/2 + i|\varkappa|) J_{-2i|\varkappa|}(-2\sqrt{-2QR_1})) \right], \end{aligned} \quad (88)$$

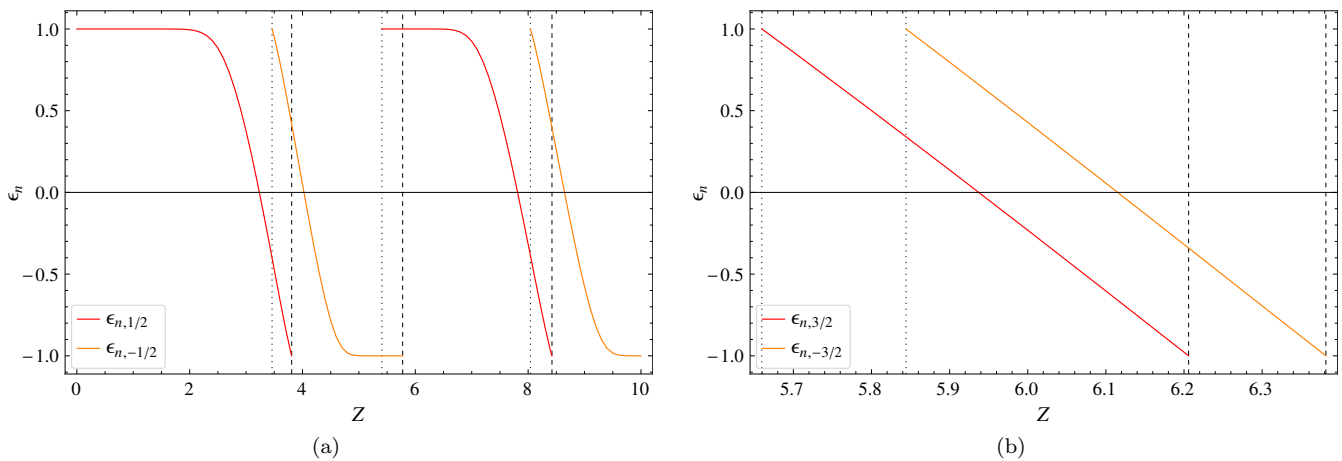


FIG. 5: (Color online) The evolution of discrete levels by growing Z for $\alpha = 0.4$, $R_0 = 1/15$, $R_1 = 2R_0$ and (a) $|m_j| = 1/2$, (b) $|m_j| = 3/2$. The vertical dashed lines denote the positions of the lower critical charges, when the levels approach the lower threshold, while the dotted ones — the moments of transformation of virtual levels into the real ones at the upper threshold.

$$\begin{aligned}
D_0(Q, R_1) = & -\frac{1}{\sqrt{2QR_1}} \frac{1}{6R_1} \text{Im} \left[\frac{1}{2} \sqrt{-2QR_1} J_{-2i\kappa}(-2\sqrt{-2QR_1}) \times \right. \\
& \times \left\{ 2(3 + 7Q^2 + 2i\kappa(3 + 4Q^2)) J_{1+2i\kappa}(2\sqrt{-2QR_0}) - \right. \\
& - \left(6 - 4Q^2 + 3(1/2 - i\kappa)V_0 + 4QR_0(1 + 3V_0) \right) \sqrt{-2QR_0} J_{2i\kappa}(2\sqrt{-2QR_0}) \left. \right] J_0(R_0\sqrt{V_0(V_0 - 2)}) + \\
& + \left[4(6 + 2QR_0 - 4Q^2(V_0 - 1) - 3V_0) J_{1+2i\kappa}(2\sqrt{-2QR_0}) - \right. \\
& - \left. \left(2 + 2V_0 - 3V_0^2 + 4i\kappa(2V_0 - 1) \right) \sqrt{-2QR_0} J_{2i\kappa}(2\sqrt{-2QR_0}) \right] \frac{QJ_1(R_0\sqrt{V_0(V_0 - 2)})}{\sqrt{V_0(V_0 - 2)}} \left. \right\} + \\
& + i\sqrt{2V_0} B_0(Q) \left(2R_1(3 + 4Q^2 - 2QR_1) J_{1-2i\kappa}(-2\sqrt{-2QR_1}) - \right. \\
& \left. - (3Q(1 + R_1^2) + 2R_1(i\kappa - 1)) \sqrt{-2QR_1} J_{-2i\kappa}(-2\sqrt{-2QR_1}) \right) \left. \right] + C_0(Q, R_1) (\gamma_E + \ln(R_1/2)) , \quad (89)
\end{aligned}$$

with γ_E being the EulerGamma.

The critical charges in this case coincide with zeros of the function $A_0(Q, R_1)$, since at the lower threshold $\gamma \rightarrow 0$ and so the equation (85), multiplied by γ^2 , takes the form $QA_0 + m_j A_0 \gamma + C_0 \gamma^2 \ln \gamma + D_0 \gamma^2 = 0$, whence it follows that $A_0(Q, R_1)$ should vanish. In its turn, the equation $A_0(Q, R_1) = 0$ is completely equivalent to the equation (71) for the corresponding lower critical charges (up to the complex conjugation).

To the contrary, for levels with $m_j = -1/2$ the expansion of the corresponding equation (74) for $\epsilon \rightarrow -1$

by keeping the leading terms containing $\gamma^{-1} \ln \gamma$ and γ^{-1} and omitting the next-to-leading ones, starting from $\ln \gamma$, yields an equation, which allows for a simple analytic solution of the form

$$\epsilon = -\sqrt{1 - C^2(Q, R_1)} , \quad (90)$$

with the function $C(Q, R_1)$ being determined by the following expression

$$C(Q, R_1) = \frac{2}{R_1} \exp \left(\frac{\text{Im} [B(Q)(\sqrt{-2QR_1} J_{1-2i|\kappa|}(-2\sqrt{-2QR_1}) + (m_j - i|\kappa|) J_{-2i|\kappa|}(-2\sqrt{-2QR_1}))]}{2QR_1 \text{Im} [B(Q) J_{-2i|\kappa|}(-2\sqrt{-2QR_1})]} - \gamma_E \right) , \quad (91)$$

$$B(Q) = Q\sqrt{1 - \frac{2}{V_0}} J_{2i|\varkappa|}(2\sqrt{-2QR_0}) J_0(R_0\sqrt{(V_0 - 2)V_0}) + (\sqrt{-2QR_0} J_{1+2i|\varkappa|}(2\sqrt{-2QR_0}) - (1/2 + i|\varkappa|) J_{2i|\varkappa|}(2\sqrt{-2QR_0})) J_1(R_0\sqrt{(V_0 - 2)V_0}). \quad (92)$$

In this case the lower critical charges correspond to the zeros of the denominator in the exponent in the expression for $C(Q, R_1)$ (91). Again, the latter precisely coincides with the equation for critical charges in this channel (72) (up to the complex conjugation).

The origin of such apparent difference in behavior of levels with $m_j = \pm 1/2$ by approaching the thresholds of continua, which is clearly seen in Fig.5a, lies in the different structure of approximate equations (85) and (90) and hence, of their solutions. Namely, the r.h.s. of (90) contains an exponent in the function $C(Q, R_1)$, which decreases very rapidly, when Z approaches the corresponding Z_{cr} . As a consequence, for $R_1 = 2R_0$ in the vicinity of the first $Z_{cr} = 5.7757028739\dots$ in the channel with $m_j = -1/2$ the level very quickly takes on values close to $\epsilon = -1$. In particular, for $Z = Z_{cr} - 1/10$ one obtains $1 + \epsilon \simeq 10^{-45}$, for $Z = Z_{cr} - 1/100$ the level lies much closer $1 + \epsilon \simeq 10^{-474}$, while for $Z = Z_{cr} - 1/1000$ the difference should be already estimated as $1 + \epsilon \simeq 10^{-4757}$. To the contrary, for $m_j = 1/2$ with the same screening in the vicinity of the first $Z_{cr} = 3.8081947856\dots$ in the channel for $Z = Z_{cr} - 1/100$ the position of the level is estimated as $1 + \epsilon \simeq 10^{-2}$, while for $Z = Z_{cr} - 1/1000$ one finds only $1 + \epsilon \simeq 10^{-3}$. This is the reason, why the

slopes of curves for levels with $m_j = \pm 1/2$ by approaching the thresholds turn out to be substantially different. Indeed here, in these estimates, the benefit of approximate equations (85) and (90) is manifested most clearly, since they allow to monitor the position of the levels even in the case when the latter are located extremely close, e.g., $\simeq -1 + 10^{-4757}$, to the threshold.

It is worth to note that such exponentially slow approach of levels in the channel with $m_j = -1/2$ to the lower threshold and with $m_j = 1/2$ to the upper one reflects in fact the well-known feature of the two-dimensional non-relativistic quantum-mechanical well, in which at least one exponentially shallow discrete level $\epsilon_{0,1/2}$ exists for arbitrary small well parameters in the partial channel with $m_j = 1/2$ (the only condition is the convergence of the integral $\int dr rU(r)$) [40]. In our DC problem the position of such a level for small Z near the upper threshold is defined by the relation, quite similar to (90)-(91)

$$\epsilon_{0,1/2} = \sqrt{1 - \tilde{C}^2(Q, R_1)}, \quad (93)$$

where

$$\tilde{C}(Q, R_1) = \frac{2}{R_1} \exp \left[\frac{F(-\varkappa, R_1)\tilde{B}(-\varkappa) - F(\varkappa, R_1)\tilde{B}(\varkappa)}{2QR_1(J_{2\varkappa}(2\sqrt{2QR_1})\tilde{B}(-\varkappa) - J_{-2\varkappa}(2\sqrt{2QR_1})\tilde{B}(\varkappa))} - \gamma_E \right], \quad (94)$$

$$F(\varkappa, R_1) = \sqrt{2QR_1} J_{1-2\varkappa}(2\sqrt{2QR_1}) - (1/2 - \varkappa) J_{-2\varkappa}(2\sqrt{2QR_1}), \quad (95)$$

$$\tilde{B}(\varkappa) = Q\sqrt{1 + \frac{2}{V_0}} J_{2\varkappa}(2\sqrt{2QR_0}) J_0(R_0\sqrt{(V_0 + 2)V_0}) + (\sqrt{2QR_0} J_{1+2\varkappa}(2\sqrt{2QR_0}) - (1/2 + \varkappa) J_{2\varkappa}(2\sqrt{2QR_0})) J_1(R_0\sqrt{(V_0 + 2)V_0}). \quad (96)$$

For $R_0 = 1/15$, $R_1 = 2R_0$, $\alpha = 0.4$ the behavior of this level on the interval $0 < Z\alpha < m_j$ is shown in Fig.6a, while in Fig.6b its dependence on the cutoff R_1 on the interval $R_0 < R_1 < 500R_0$ is given for $Z = 1/10$. For $R_1 \rightarrow \infty$ it transforms into the lowest discrete level in this partial channel for the unscreened case with the limiting value $\epsilon_{0,1/2} \simeq 0.996828726314219\dots$. From Figs.6a,b there follows that for Z very close to zero there exists always one discrete level $\epsilon_{0,1/2}$ with $m_j = 1/2$, which with decreasing Z tends very rapidly to 1. In particular, for our standard set of parameters $R_0 = 1/15$, $R_1 = 2R_0$,

$\alpha = 0.4$ and $Z = 1/10$ one has $\epsilon_{0,1/2} \simeq 1 - 10^{-107}$, whereas for $Z = 1/100$ it lies already at $\simeq 1 - 10^{-1084}$. Indeed such behavior is demonstrated by other levels with $m_j = 1/2$ just after creation at the upper threshold and with $m_j = -1/2$ by approaching the lower one for $Q > |m_j|$.

Another peculiar feature of the channels with $|m_j| = 1/2$ and $|m_j| = 3/2$ is the behavior of the induced density by crossing the lower Z_{cr} , since in this case the Fano rule in the form (40) for $\Delta\rho_{VP}(r)$ doesn't work. Nevertheless, the jump in the density by crossing the lower threshold

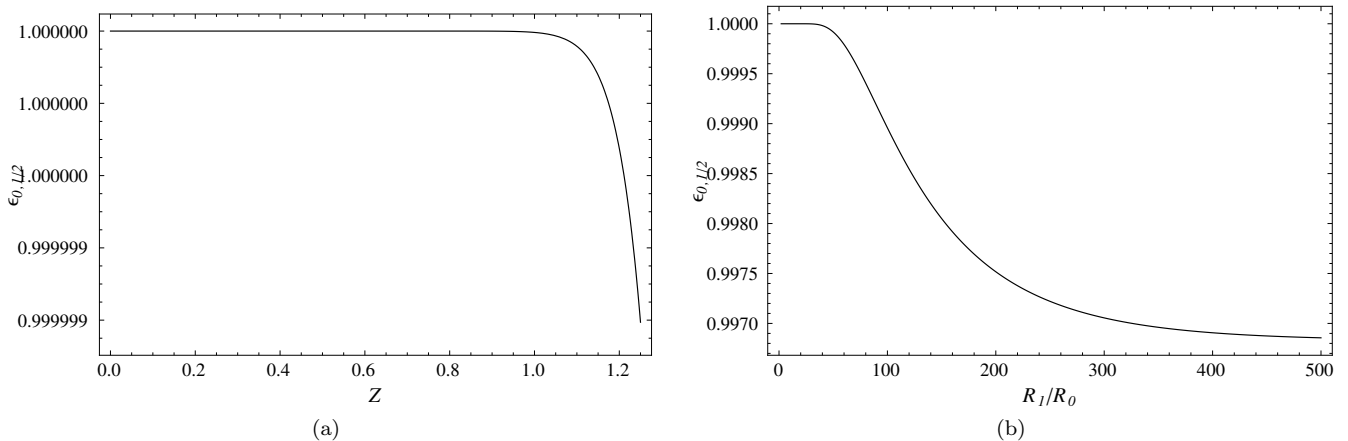


FIG. 6: (a): The behavior of the first discrete level $\epsilon_{0,1/2}$ as a function of the source charge Z for $\alpha = 0.4$, $R_0 = 1/15$, $R_1 = 2R_0$; (b): the dependence of the level $\epsilon_{0,1/2}$ on the cutoff R_1 for $\alpha = 0.4$, $R_0 = 1/15$ and $Z = 1/10$.

can be well understood by taking into account that the non-normalizable solutions (70) and (81) appear as the limiting behavior of corresponding discrete levels for $\epsilon \rightarrow -1$, and so instead of (40) we get

$$\Delta\rho_{VP}(r) = -2|e| \lim_{\epsilon_n \rightarrow -1} \psi_{n,m_j}(r)^\dagger \psi_{n,m_j}(r). \quad (97)$$

In particular, the jump in the induced density distribution by diving of the corresponding level with $|m_j| = 1/2$ and $m_j = -3/2$ into the lower continuum turns out to be the (improper) limit of normalizable distributions spread over the whole half-axis $0 \leq r \leq \infty$, which carries with an amount $(-2|e|)$ of the total induced charge. The latter result is well verified via direct numerical calculation. The behavior of the jumps in the induced density depending on ΔZ by crossing the lower threshold are shown in Figs.7a,c,e for $m_j = 1/2$ and in Fig.7b,d,f for $m_j = -3/2$. In these figures the difference between induced densities taken at $Z_{cr} - \Delta Z/2$ and $Z_{cr} + \Delta Z/2$ for decreasing ΔZ is presented. As it was already stated in Section 3, the jumps in the induced density by levels diving into the lower continuum represent themselves the essentially non-perturbative effect, completely included in $\rho_{VP}^{(3+)}$, while $\rho_{VP}^{(1)}$ does not participate in it and still makes an exactly vanishing contribution to the total induced charge. To demonstrate the effect of spreading of jumps in the induced density at the threshold more clearly, in Figs.7c,d and in Figs.7e,f the weighted densities $r \times \rho_{VP,m_j}^{(3+)}(r)$ and $r^2 \times \rho_{VP,m_j}^{(3+)}(r)$ are used. From Figs.7 it should be clear that the less is ΔZ by crossing the threshold, the more spread is the jump in the induced density distribution, but the loss of amount $(-2|e|)$ of the total induced charge remains unchanged.

6. CONCLUSION

Thus, in this work the vacuum polarization effects in the 2+1-dimensional strongly-coupled QED, caused by

diving of levels into the lower continuum, have been considered in terms of the renormalized vacuum density $\rho_{VP}^{ren}(\vec{r})$. The 2+1-dimensional case differs significantly from the one-dimensional one first of all in that $\rho_{VP}^{ren}(\vec{r})$ is represented now by an infinite series in the rotational quantum number m_j , and so there appears an additional problem of its convergence. As it was shown in [29], this problem can be successfully solved by renormalization of the vacuum density within PT, i.e. via regularization of the solely divergent fermionic loop with two external lines. Simultaneously, the integral vacuum charge vanishes automatically in the subcritical region, and is changed by $(-2|e|)$ upon diving of each subsequent doubly degenerate discrete level into the lower continuum. Such behavior of $\rho_{VP}^{ren}(\vec{r})$ in the overcritical region confirms once more the assumption of the neutral vacuum transmutation into the charged one under such conditions ([11–15] and refs. therein).

It should be noted also that in the most of works cited above [4, 17–25] the impurity potentials are considered without any kind of screening at large distances from the Coulomb source. However, in fact in such systems there should definitely exist a finite $R_1 > R_0$, beyond which the influence of the impurity charge will be negligibly small. And although the concrete form of the screened potential could be more smooth (e.g., an exponential one), already the considered peculiar effects by screening in the form of the simplest shielding via vertical wall for the lowest partial channels $|m_j| = 1/2, 3/2$ deserve special interest, since indeed the levels with such rotational numbers should first dive into the lower continuum. The most intriguing circumstance here is that the jump in the induced density by crossing the corresponding Z_{cr} can be very weakly expressed, since the change in the induced density distribution should be evenly spread over the entire surface of the sample. This effect should be especially remarkable for the levels with $m_j = -1/2$, since in this case such spreading of density will take place for a whole interval $\Delta Z \sim 1$ before reaching the corresponding Z_{cr} (see Fig.5a). Therefore, recording such a

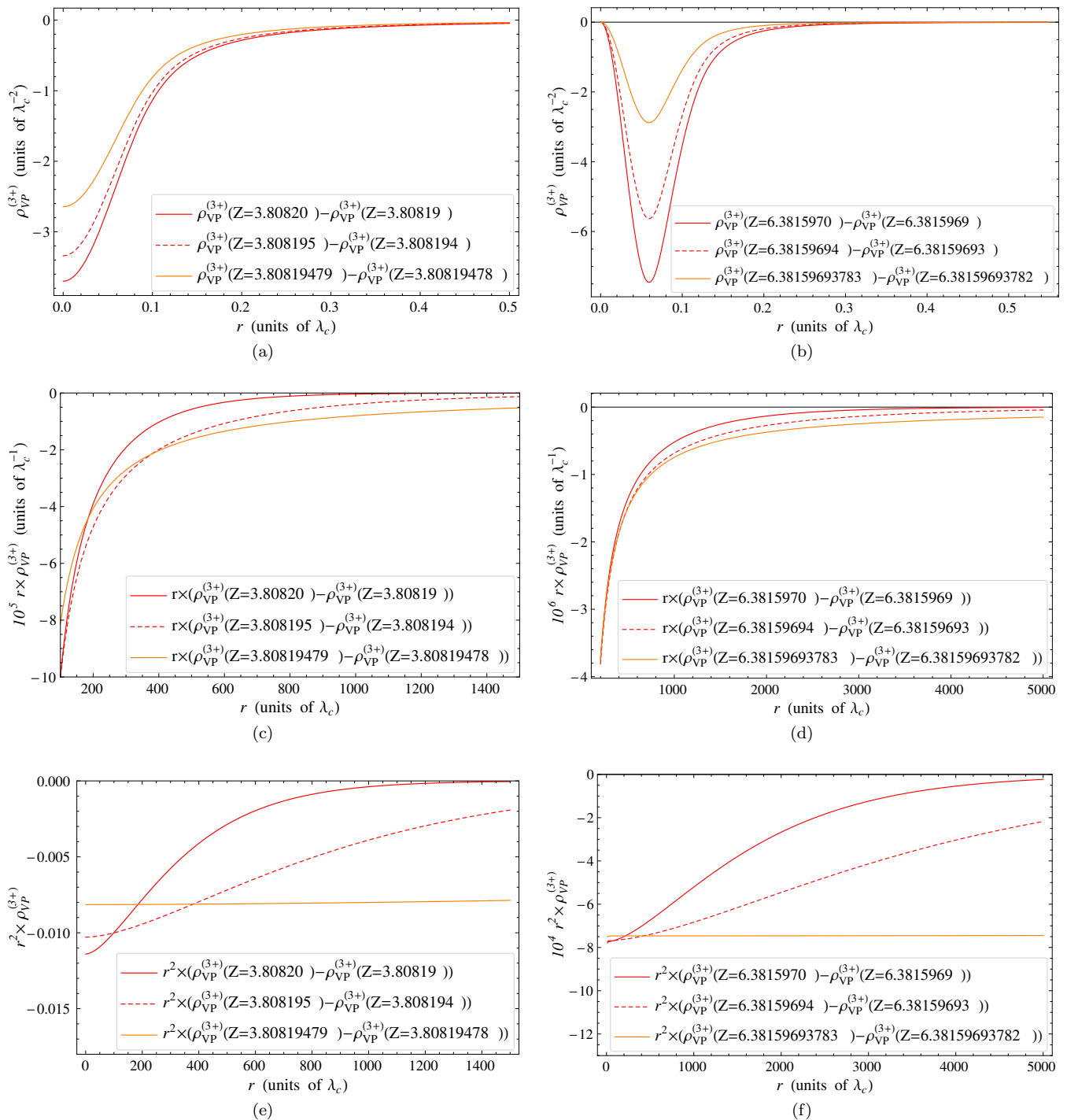


FIG. 7: (Color online) The jumps in the induced density depending on ΔZ by crossing the lower threshold for $\alpha = 0.4$, $R_0 = 1/15$, $R_1 = 2R_0$ (a), (c), (e): for $m_j = 1/2$ and (b), (d), (f): for $m_j = -3/2$.

change in the induced density can be significantly hampered, and the only reliable way of confirming the effect is to measure directly the corresponding change in the total induced charge. Such measurement, however, poses additional problems. Moreover, even for the first normalizable discrete levels at the lower threshold with $m_j = 3/2, \pm 5/2, \dots$ that provide just the required degree of decrease of the electronic WF at the radial infin-

ity, the jump in the induced density in the screened case will also be significantly smeared over the surface of the sample. So in the screened case the study of such critical effects in terms of the induced density could run into serious difficulties.

This circumstance, however, doesn't mean that the critical effects cannot be observed in the screened case at all, rather it indicates the need to study the Casimir

effects. Although the most of works cited above treats the induced charge density $\rho_{VP}(\vec{r})$ as the main polarization observable, the Casimir (vacuum) energy \mathcal{E}_{VP} turns out to be not less informative and in many respects complementary to $\rho_{VP}(\vec{r})$. Moreover, compared to $\rho_{VP}(\vec{r})$, the main non-perturbative effects, which appear in the vacuum polarization for $Z > Z_{cr,1}$ due to levels diving into the lower continuum, show up in the behavior of \mathcal{E}_{VP} even more clear, demonstrating explicitly their possible role in the overcritical region [31, 36, 41, 42]. Namely, with growing Z in the overcritical region $\mathcal{E}_{VP}^{ren}(Z)$ falls into the region of large negative values with a rate that depends on the total number of discrete levels, dived into the lower continuum. In 2+1 D the growth rate of this

number turns out to be sufficiently higher than in 1+1 D due to the contributions from different partial channels. The estimate, obtained in [29], shows that this growth rate should be not less than $\sim Z^{2.17}$. As a result, in the 2+1 D toy models considered in [31, 38], $\mathcal{E}_{VP}^{ren}(Z)$ turns out to be negative estimated as $\sim -Z^3/R_0$. Such decrease of \mathcal{E}_{VP} could significantly affect the basic properties of the considered graphene-like DC system upon doping by charged impurities with $Z > Z^* \sim O(10)$, leading to a special type of affinity between the impurities and the graphene plane. However, a rigorous evaluation of this effect requires for a substantial amount of additional calculations and numerical tools and will be reported in a separate paper.

-
- [1] A. H. Castro Neto, F. Guinea, N. M. R. Peres, K. S. Novoselov, and A. K. Geim, *Rev. Mod. Phys.* **81**, 109 (2009).
- [2] J. P. Reed, B. Uchoa, Y. I. Joe, Y. Gan, D. Casa, E. Fradkin, and P. Abbamonte, *Science* **330**, 805 (2010).
- [3] A. Shytov, M. Rudner, N. Gu, M. Katsnelson, and L. Levitov, *Solid State Communications* **149**, 1087 (2009).
- [4] A. V. Shytov, M. I. Katsnelson, and L. S. Levitov, *Phys. Rev. Lett.* **99**, 236801 (2007).
- [5] M. I. Katsnelson, K. S. Novoselov, and A. K. Geim, *Nature Physics* **2**, 620 (2006).
- [6] V. P. Gusynin and S. G. Sharapov, *Phys. Rev. Lett.* **95**, 146801 (2005).
- [7] A. Giesbers, U. Zeitler, M. Katsnelson, M. Ponomarenko, T. Mohiuddin, and J. Maan, *Physica E* **40**, 1089 (2008).
- [8] C. Cobaleda, F. Rossella, Pezzini, E. Diez, V. Bellani, D. Maude, and P. Blake, *Physica E* **44**, 530 (2011).
- [9] A. V. Shytov, M. S. Rudner, and L. S. Levitov, *Phys. Rev. Lett.* **101**, 156804 (2008).
- [10] W.-Y. He, Z.-D. Chu, and L. He, *Phys. Rev. Lett.* **111**, 066803 (2013).
- [11] W. Greiner, R. Müller, and J. Rafelski, *Quantum Electrodynamics of Strong Fields*, 2nd ed. (Springer, Berlin, 1985).
- [12] G. Plunien, B. Müller, and W. Greiner, *Phys. Rep.* **134**, 87 (1986).
- [13] R. Ruffini, G. Vereshchagin, and S.-S. Xue, *Phys. Rep.* **487**, 1 (2010).
- [14] W. Greiner and J. Reinhardt, *Quantum Electrodynamics*, 4th ed. (Springer-Verlag Berlin Heidelberg, 2009).
- [15] J. Rafelski, J. Kirsch, B. Müller, J. Reinhardt, and W. Greiner, "Probing QED Vacuum with Heavy Ions," in *New Horizons in Fundamental Physics*, FIAS Interdisciplinary Science Series (Springer, 2017) pp. 211–251.
- [16] Y. Wang, D. Wong, A. V. Shytov, V. W. Brar, S. Choi, Q. Wu, H.-Z. Tsai, W. Regan, A. Zettl, R. K. Kawakami, S. G. Louie, L. S. Levitov, and M. F. Crommie, *Science* **340**, 734 (2013).
- [17] M. I. Katsnelson, *Phys. Rev. B* **74**, 201401 (2006).
- [18] R. R. Biswas, S. Sachdev, and D. T. Son, *Phys. Rev. B* **76**, 205122 (2007).
- [19] V. M. Pereira, J. Nilsson, and A. H. Castro Neto, *Phys. Rev. Lett.* **99**, 166802 (2007).
- [20] V. N. Kotov, V. M. Pereira, and B. Uchoa, *Phys. Rev. B* **78**, 075433 (2008).
- [21] I. S. Terekhov, A. I. Milstein, V. N. Kotov, and O. P. Sushkov, *Phys. Rev. Lett.* **100**, 076803 (2008).
- [22] Y. Nishida, *Phys. Rev. B* **90**, 165414 (2014).
- [23] V. R. Khalilov and I. V. Mamsurov, *Phys. Lett. B* **769**, 152 (2017).
- [24] M. M. Fogler, D. S. Novikov, and B. I. Shklovskii, *Phys. Rev. B* **76**, 233402 (2007).
- [25] A. I. Milstein and I. S. Terekhov, *Phys. Rev. B* **81**, 125419 (2010).
- [26] V. M. Pereira, V. N. Kotov, and A. H. Castro Neto, *Phys. Rev. B* **78**, 085101 (2008).
- [27] M. O. Goerbig, *Rev. Mod. Phys.* **83**, 1193 (2011).
- [28] H. Sadeghi, S. Sangtarash, and C. Lambert, *Physica E* **82**, 12 (2016).
- [29] A. Davydov, K. Sveshnikov, and Y. Voronina, *Int. J. Mod. Phys. A* **33**, 1850004 (2018).
- [30] P. J. Mohr, G. Plunien, and G. Soff, *Phys. Rep.* **293**, 227 (1998).
- [31] A. Davydov, K. Sveshnikov, and Y. Voronina, *Int. J. Mod. Phys. A* **33**, 1850005 (2018).
- [32] E. H. Wichmann and N. M. Kroll, *Phys. Rev.* **101**, 843 (1956).
- [33] Y. Hosotani, *Phys. Lett. B* **319**, 332 (1993).
- [34] H. Bateman and A. Erdelyi, *Higher Transcendental Functions*, Vol. 1-2 (Mc Graw-Hill, New York, 1953).
- [35] M. Gyulassy, *Nucl. Phys. A* **244**, 497 (1975).
- [36] A. Davydov, K. Sveshnikov, and Y. Voronina, *Int. J. Mod. Phys. A* **32**, 1750054 (2017).
- [37] U. Fano, *Phys. Rev.* **124**, 1866 (1961).
- [38] K. Sveshnikov, Y. Voronina, A. Davydov, and P. Grashin, submitted to *Theor. Math. Phys.* (2018).
- [39] Y. Voronina, K. Sveshnikov, A. Davydov, and P. Grashin, arXiv:1802.05336 [cond-mat.mes-hall] (2018).
- [40] L. Landau and E. Lifshitz, "Quantum mechanics non-relativistic theory, third edition: Volume 3 (course of theoretical physics) (vol. 3) 3rd edition," (Pergamon Press, NY, 1981) pp. 1–673.
- [41] Y. Voronina, A. Davydov, and K. Sveshnikov, *Theor. Math. Phys.* **193**, 1647 (2017).
- [42] Y. Voronina, A. Davydov, and K. Sveshnikov, *Phys. Part. Nucl. Lett.* **14**, 698 (2017).